The Role and Dynamics of Oxygen Of Ionospheric Origin in Magnetopause Reconnection

Kevin J. Genestreti[1,2]

In collaboration with:

L. M. Kistler[1] and C. G. Mouikis[1]

A thesis submitted for the degree of

Bachelor of Science

Spring, 2012

[1] Space Science Center, University of New Hampshire, Durham, NH
[2] Undergraduate, Department of Physics, UNH, Durham, NH

Table of Contents

1. Abstract

In this study we analyze the dynamics of ionized oxygen (O^+) of ionospheric origin in magnetopause reconnection events. We seek to determine whether or not the large gyroradius of O^+ inhibits its coupling to the reconnection region. In order to do so, we analyze the properties of the magnetopause boundary layer and the dynamics of the nearby ions using Cluster/CODIF and magnetometer data. To identify reconnection events we use minimum variance analysis and the Walén relation to demonstrate that the properties of the ions and fields at the magnetopause are consistent with those of a locally, rotationally discontinuous boundary. In order to better understand the role of O^+ in magnetopause reconnection, we present detailed case studies where O^+ is observed in reconnection jet encounters. For four separate jets in two distinct events we find O^+ to be either fully or partially magnetized and streaming close to the velocity predicted by the Walén relation. We also estimate the normalized reconnection rate for two of the four reconnection encounters using the relationship $B_N \,/\, B_L \cong R_{NORM}$ and find a nominal normalized rate of ~0.1 for each. In the concluding remarks, we discuss ways that this study may be broadened to estimate the impact of O^+ on the various parameters of magnetopause reconnection.

2. Introduction

Magnetic reconnection is the vehicle through which magnetized plasmas expel magnetic energy into particle kinetic energy. The conditions necessary to initiate magnetic reconnection are found commonly in plasmas throughout the universe; in these various regimes of plasmas reconnection is thought to a common process for driving such energy exchange. It is a mechanism that has been used to explain the generation of solar flares (*Giovanelli* et al., [1947]), high-energy bursts on magnetized neutron stars (*Somov et al.*, [2003]) and many phenomena observed in the Earth's magnetosphere/ionosphere (*Dungey*, [1961]). Near Earth, reconnection is known to be an important link in the chain of events which generates auroral events and geomagnetic storms (Many papers, e.g. several by Dungey, 1950's). It is also considered to be the main mechanism which allows for mass, energy and momentum flux across the boundary between the Earth's magnetic field and the solar wind (*Paschmann et al.,* [1979]). Studying reconnection in the Earth's magnetosphere is considered important for two reasons:

1. Developing an understanding of reconnection is a necessary perquisite to building a description of our own near-Earth environment
2. Studying reconnection close to home allows for the inference of a universal physical process with relative ease.

Yet while the importance of reconnection is well established and observational evidence of reconnection has been present for some time[1], there are still many gaps in the current understanding of reconnection physics. There are many unanswered questions regarding what determines the structure of the reconnection region and the rate at which reconnection occurs.

One such unanswered question is what role, if any, ionized oxygen (O^+) has in determining on the reconnection rate and structure. The O^+ content observed in the

[1] Evidence consists of ISEE observations of the magnetopause as a rotational discontinuity (*Sonnerup et al.,* [1981]), ISEE observations of ion flows following signatures of jump conditions of a rotational discontinuity (*Paschmann et al.,* [1979]), observations of 'D-shaped' ion distributions (*Gosling et al.,* [1990]), and ground-based observations of ionospheric phenomena coinciding with reconnection theory (*Lockwood and Smith,* [1996]).

magnetosphere is highly variable. It is prone to drastic intensifications during times of heightened geomagnetic activity (*Mouikis et al.,* [2010]). Due to the large mass of O^+ compared to protons (H^+) this variability in O^+ content can generate large variations in the total mass density of the magnetospheric plasma. The effects of O^+ on reconnection and the dynamics of O^+ in the reconnection region are not well understood. It is also not well understood whether or not O^+ is involved in reconnection. In this study we seek to experimentally address the influence that O^+ has on reconnection dynamics. We will demonstrate that O^+ is in fact involved with reconnection. We will focus specifically on reconnection at the Earth's magnetopause.

So far, relatively few experimental analyses have considered heavy ions in the description of reconnection physics. Observations have been made of heavy ions, such as oxygen, present during reconnection events (*Chaston et al.,* [2005], *Phan et al.,* [2003]). Other large scale statistical studies have but none provide the detailed analysis necessary to determine their level of involvement in the reconnection process. Theoretical work has been done to simulate the effects of heavy ions on magnetic reconnection but many of these studies draw contradicting conclusions (*Hesse and Birn,* [2004], *Swisdak and Shay*, [2004], *Karimabadi et al.,* [2011]). So far this question remains unknown. This study will present observational evidence that O^+ participates in reconnection related acceleration, the initial step to showing that O^+ may have an effect on determining reconnection dynamics.

3. Theory

3.1. The Basic Geometry of Magnetic Reconnection

Figure 1 displays a simplified geometry of reconnection in set of three still frames. In Figure 1a, a loading of magnetic pressure and an increased current along a boundary forces two opposing magnetic fields to pinch together at a point. In Figure 1b, the two opposing magnetic fields meet and reconnect with one another, releasing large amounts of magnetic energy. This energy heats and accelerates the nearby plasmas contained in magnetic fields B_1 and B_2. These plasmas are now free to diffuse and cross the current sheet boundary layer. In the transition from Figures 1b to 1c, the fields forming the X-line structure have undergone reconnection. In Figure 1c these field lines are bent sharply. The tension stored in the bent magnetic field lines causes them to forcibly straighten out. This is observed as a 'snapping back' of the field lines and away from the plasma diffusion region to the north and south of the magnetic null point. The convecting field lines carry the diffusing plasmas with them. In Figure 1c plasma inflow is drawn from the left and right of the reconnection region to be convected away in jets to the top and bottom of the diffusion region. In the transition between Figures 1a and 1c, the topology of the boundary layer between fields B_1 and B_2 has been entirely reconfigured. In Figure 1a, the boundary is closed and plasmas and magnetic field lines are not able to diffuse across it. This type of boundary structure is called a 'tangential discontinuity'. In Figure 1c, the boundary is open and nonzero fluxes of magnetic field lines and plasma occurs readily across it. This type of boundary is called a 'rotational discontinuity' and is generated by reconnection (*Levy et al.,* [1964]). The identification of boundaries of this type will be used to aid the identification of reconnection events, using methodology described in *Section* **5. Methodology***.*

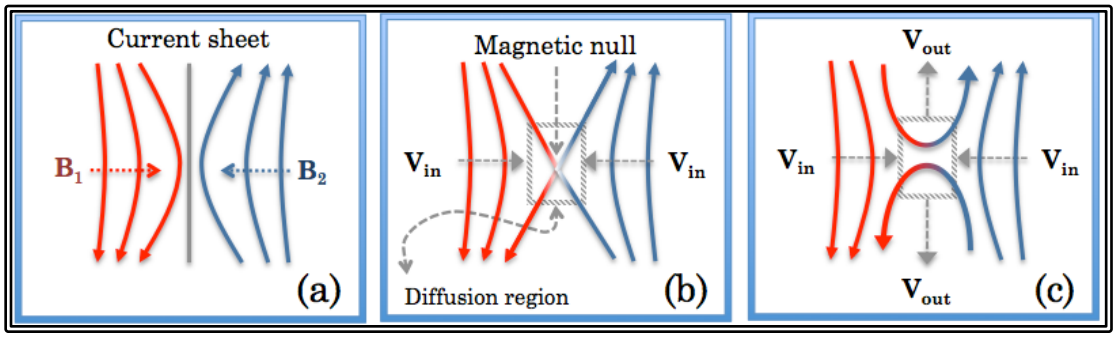

Figure 1: A two-dimensional depiction of the geometry of magnetic reconnection. In frame (a) two magnetic fields bounded by a current sheet pinch together. In frame (b) the two fields reconnect. In frame (c) the newly reconnected field lines convect away carrying plasma with them.

Reconnection is observed primarily in two regions of the magnetosphere, namely the magnetopause and the magnetotail current layers (*Kivelson and Russell*, "Intro. to Space Phys.": The Magnetopause, Magnetotail and Mag. Reconnection). In both of these regions the antiparallel field configuration shown in Figure 1a is commonly observed, suggesting magnetic reconnection is a common occurrence. For the case of magnetopause reconnection, the two fields are those of the Earth and the solar wind. Figure 2 shows the magnetosphere, the solar wind / interplanetary magnetic field (IMF) and the expected locations of magnetic reconnection (*Kivelson and Russell*, "Intro. to Space Phys.": The Magnetopause, Magnetotail and Magnetic Reconnection, [1995]). The case shown in Figure 2 is that where the IMF is almost fully southward. Under these IMF conditions, reconnection at the magnetopause is expected to occur at the subsolar point (the point on the magnetopause closest to the sun).

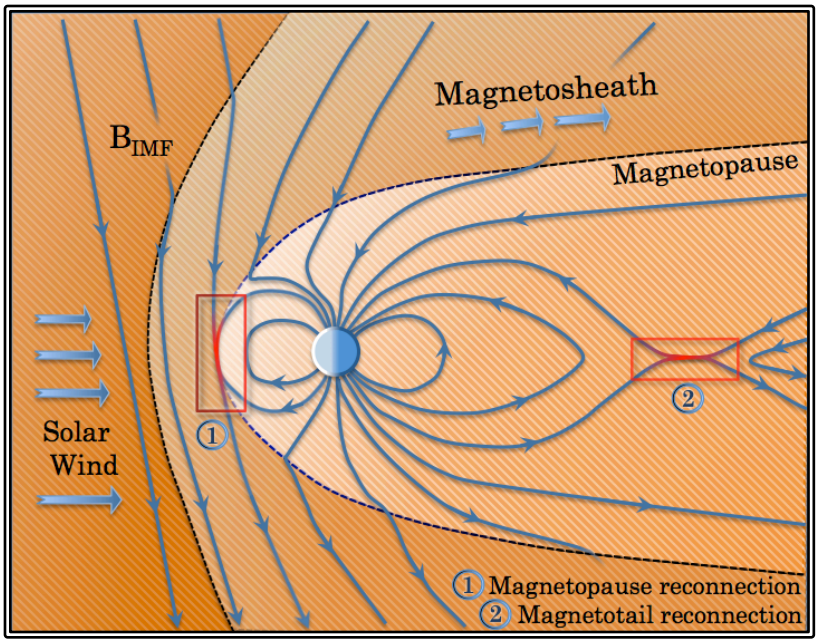

Figure 2: The locations in the Earth's magnetosphere where reconnection is considered a common occurrence. The solar wind and magnetosheath plasma flows are also shown. Figure adapted from *Kivelson and Russell*, "Introduction to Space Physics", Fig. 9.11.

3.2. The Magnetopause Boundary Layer

The magnetopause is the outermost extent of the Earth's magnetic field. It separates the terrestrial field and magnetospheric plasma from the IMF and shocked solar wind (magnetosheath) plasma. Under typical conditions, meaning without reconnection, the magnetopause boundary is a closed and tangentially discontinuous boundary. It is also a current layer, like most plasma boundaries in space (*Kivelson and Russell*, "Intro. to Space Phys.": The Magnetopause, Magnetotail and Magnetic Reconnection, [1995]). Solar wind impacting the magnetosphere experiences a Lorentz $q\vec{v}\times\vec{B}$ force, where q is the charge of a particle, $\vec{v}$ is the velocity, and $\vec{B}$ is the magnetic field. Note that the direction of the force is dependent on charge. It is this separation of charge that generates the magnetopause current. Figure 3 illustrates the trajectory and deflection of solar wind particles that occurs at the magnetopause during times when reconnection is not occurring (i.e. the magnetopause is a tangential discontinuity). A typical thickness of the magnetopause (as a tangential discontinuity) is between 100-4000 km (*Berchem and Russell,* [1982]).

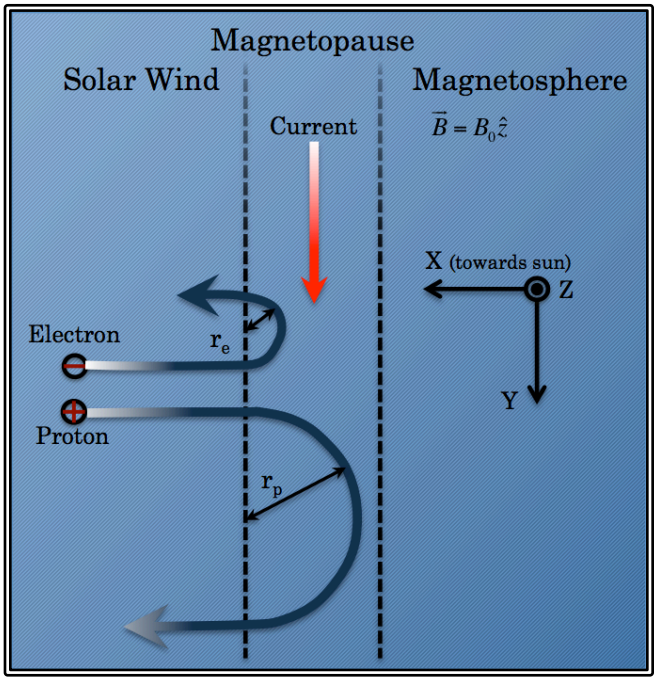

Figure 3: Trajectories of solar wind particles as they encounter the magnetopause at the subsolar point. Conditions depicted here are those where reconnection is not occurring, and the magnetopause is a tangential discontinuity. Figure adapted from *Kivelson and Russell*, "Introduction to Space Physics", Fig. 9.2.

The location of the magnetopause boundary is determined by the pressure balance between the terrestrial field (mainly magnetic pressure) and by the magnetosheath plasma (mainly dynamic pressure). The location of the magnetopause is variable and it will actively readjust its three-dimensional structure to balance variations in the solar wind dynamic pressure (*Kivelson and Russell*, "Intro. to Space Phys.": The Magnetopause, Magnetotail and Magnetic Reconnection, [1995]).

As shown in Figure 2, the magnetopause is the boundary between the magnetosheath and magnetospheric plasmas. The magnetosheath plasma consists mostly of H^+, He^{++} and e^- at warm temperatures and high densities. The magnetosheath plasma flows around the Earth, as shown in Figure 2. This generates shear stresses at the magnetopause boundary. The plasma on the magnetospheric side of the magnetopause consists mainly of H^+ and e^- with a variable presence of O^+ and He^+ depending on the level of geomagnetic activity. The magnetospheric plasma

consists of hot, sparse plasma. There is also a secondary cold plasma population in the magnetosphere which upwells from the plasmasphere. Though both populations may contain O^+, our focus is on the hotter population. Measurement of plasma with such low temperatures (≤1keV) is difficult with electrostatic analyzer-based instrumentation and requires the use of imaging spectroscopy (NASA Webpage: TWINS Mission) or retarding potential analysis (*McCarthy et al.,* [1998]).

3.3. Ionospheric Oxygen In the Magnetosphere

O^+ is a unique constituent of the near-Earth plasma because it, unlike most other species, originates almost entirely from the Earth rather than the solar wind. O^+ outflows from the cusp along two primary transport paths, as shown in Figure 4 (*Liu,* Ph.D. Thesis Proposal, [2012]). In the dayside polar cusp, ultraviolet radiation from the sun ionizes and energizes oxygen in the uppermost reaches of the atmosphere. The energized oxygen then streams outward along the open field lines in the cusp. It is then transported tailward where it is eventually deposited into the distant magnetotail (red arrow, Figure 4). The O^+ outflow along the dayside cusp is thought to be a relatively consistent feature, though it has been found to vary with the geomagnetic conditions and the F10.7 index, a proxy of the ionizing UV radiation from the sun (*Mouikis et al*., [2010]).

O^+ may also outflow from the nightside auroral zone. The nightside auroral outflow is prone to drastic intensifications during times of high geomagnetic activity. This path transports O^+ directly into the tail plasma sheet, where it will convect sunward back into the inner magnetosphere (dark blue arrows, Figure 4). Surveys of the tail plasma sheet have observed dependence have observed dependence on O^+ content on the Kp index a proxy for the level of geomagnetic activity (*Mouikis et al.,* [2010]). In some cases, O^+ was even found to dominate the total number density of the plasma (*Kistler et al*., [2005]). Depending on the path of convection of the O^+ from the tail plasma sheet, it will come to populate either the plasma in the inner magnetosphere and radiation belt or the magnetospheric plasma along the magnetopause. O^+ originating from nightside auroral outflow is typically observed at high energies consistent with those of the tail plasma sheet.

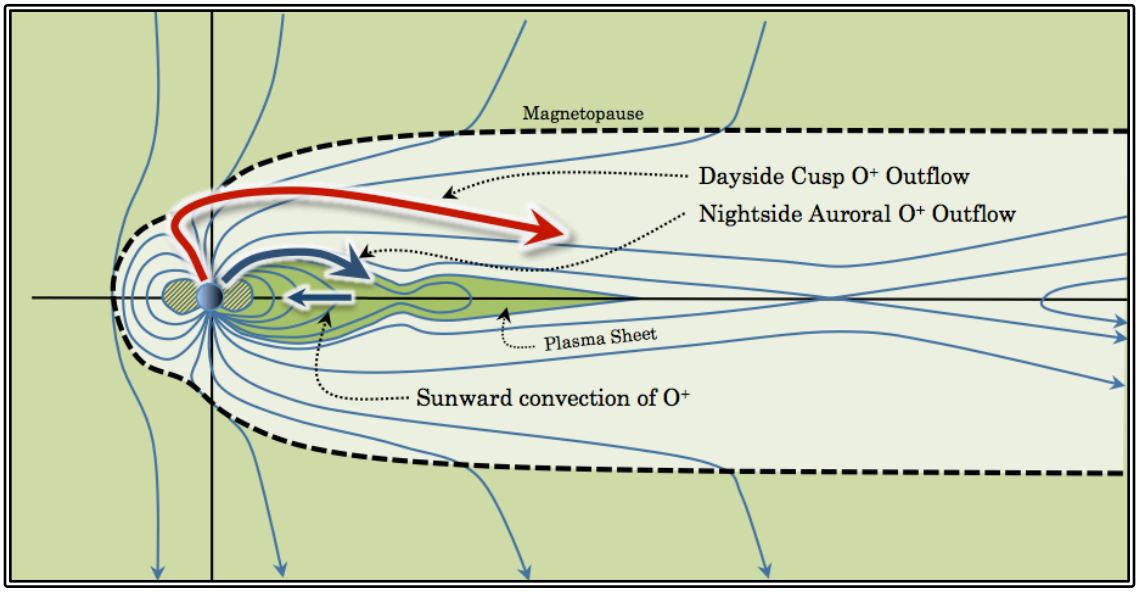

Figure 4: Transport path of oxygen from the ionosphere to the inner magnetosphere. Figure adapted from *Kivelson and Russell*, "Introduction to Space Physics", Fig. 13.22.

In a large statistical study, O^+ was observed to range from a minor to the majority contributor to the plasma mass density on the magnetospheric side of the magnetopause (*Bourham et al.,* [2005]). For this reason, and because the degree of O^+ content at the magnetopause is highly variable, studying O^+ in magnetopause reconnection may be crucial to building a complete understanding of the process as a whole.

3.4. The Finite Gyroradius Effect

In a magnetic field, charge particles will undergo gyration according to the Lorentz $q\vec{v}\times\vec{B}$ force. The radius of gyration is given by Equation (1), where r_c is the radius of gyration, m is the mass of the particle, $v_\perp$ is the velocity perpendicular to the magnetic field, q is the charge of the particle and B is the magnetic field strength.

$$r_c = \frac{mv_\perp}{qB} \tag{1}$$

Note that r_c is dependent on both mass and velocity and inversely proportional to the magnetic field strength. Given relatively weak magnetic fields, like those within the reconnection region, and high energy and high mass particles, like energetic O^+,

the value of r_c becomes relatively large if compared to the width of the magnetopause boundary. When this happens, leakage may occur as O^+ gyrates across the boundary.

MHD, the treatment of plasmas as a magnetized fluid, is only accurate on spatial scales much larger than the gyroradii of the plasma. Since boundaries such as the magnetopause are formed on spatial scales comparable to the gyroradii of heavy ions, the finite gyroradius effect may be described as a breakdown of MHD, and subsequently as a breakdown of the "frozen-in condition" which falls out of MHD. The importance of the "frozen-in condition" in determining reconnection dynamics and further explanation of the effects of the finite gyroradius of O+ will be discussed in *Section* ***Error! Reference source not found.***.

3.5. Magnetopause Reconnection

As shown in Figure 2, the magnetopause bounds the solar wind IMF and magnetospheric field. Reconnection may occur between these two fields if their orientation relative to one another is at least semi-antiparallel (*Fuselier et al.,* [2011]). Although Figure 2 shows the specific case of southward IMF generating reconnection at the subsolar point, reconnection will occur under a variety of IMF orientations at a variety of locations along the three-dimensional magnetopause[1]. The location of reconnection is determined by where along the boundary the antiparallel field geometry is generated (*Crooker*, [1979]). (For completeness it bears mentioning that a recent empirical model suggests that component reconnection, or semi-antiparallel reconnection, may be favored under certain IMF orientations (*Trattner et al.,* [2007]).)

Figure 5 shows a larger depiction of a magnetopause reconnection event. Note the mixture of plasmas which occurs across the magnetopause. This plasma flux allows the dense, warm magnetosheath plasma to enter into the magnetospheric cavity and allows the escape of the magnetospheric plasma.

[1] For instance, the events studied in *Lindstedt et al.,* An. Geophys., [2009], *Vaivads et al.,* PRL, [2004] and *Fuselier et al.,* JGR, [2005] observed magnetopause reconnection at various MLT / latitudes during times with different IMF orientations.

Ionospheric O^+ located on the magnetospheric side of the magnetopause may escape across the magnetopause in one of two ways:

1. If O^+ participates in reconnection, it may be able to cross the boundary by means of reconnection related acceleration
2. O^+ may leak across the reconnection region due to the finite gyroradius effect.

Many studies, including this one, have observed O^+ outside the magnetopause. Some of those studies concluded that the O^+ finite gyroradius effect was likely the source of its escape (*Marcucci et al.,* [2004]), others concluded that reconnection was likely the source for the escape (*Zong et al.,* [2001], *Kistler et al.,* [2005], *Wygant et al.,* [2005], *Kasahara et al.,* [2008]). Part of this study will be determining whether or not O^+ can participate in reconnection, subsequently determining whether process 1, above, is a viable mechanism for O^+ escape from the magnetosphere.

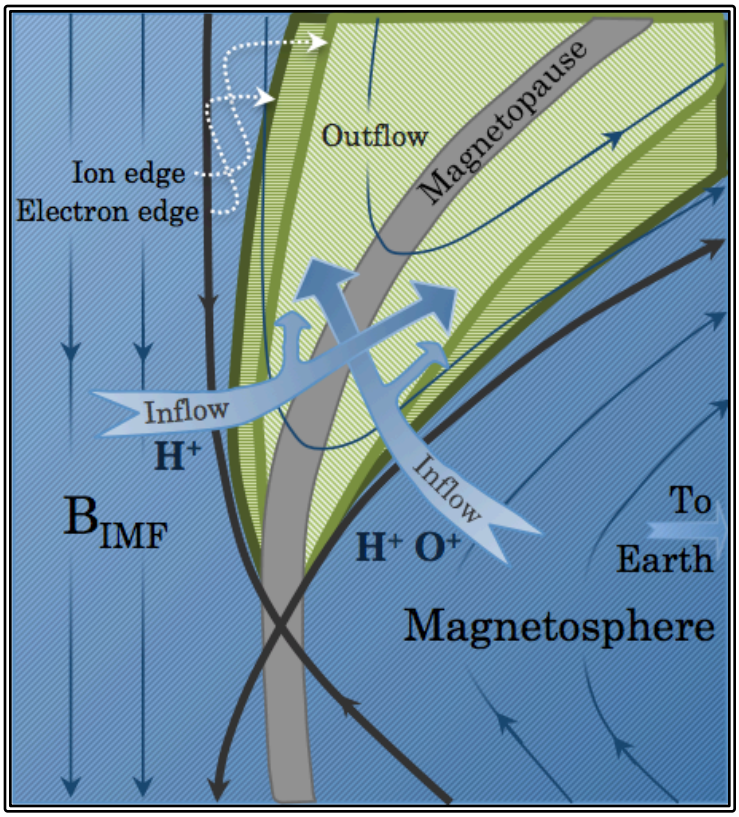

Figure 5: Reconnection at the magnetopause. The magnetopause is shown in light grey, the actively reconnecting field lines are shown in dark grey, the outflow regions of ions and electrons are the areas shaded in light and dark green and the boundaries of these outflow regions are the lines of similar color. Figure adapted from *Gosling et al.*, [1990].

3.6. Detail of the Reconnection Region

Figure 6 shows the geometry of the fields and plasma flows in the reconnection region in greater detail than Figures 1 and 5. Here the dynamic Hall electromagnetic fields are shown. The asymmetric field geometry shown in Figure 5, which is characteristic of magnetopause reconnection, has been ignored here for the sake of simplicity. This figure is limited in the sense that it only describes fully antiparallel and symmetric reconnection. In each of the four corners of the image, the directions of the magnetic field and plasma flows have been included.

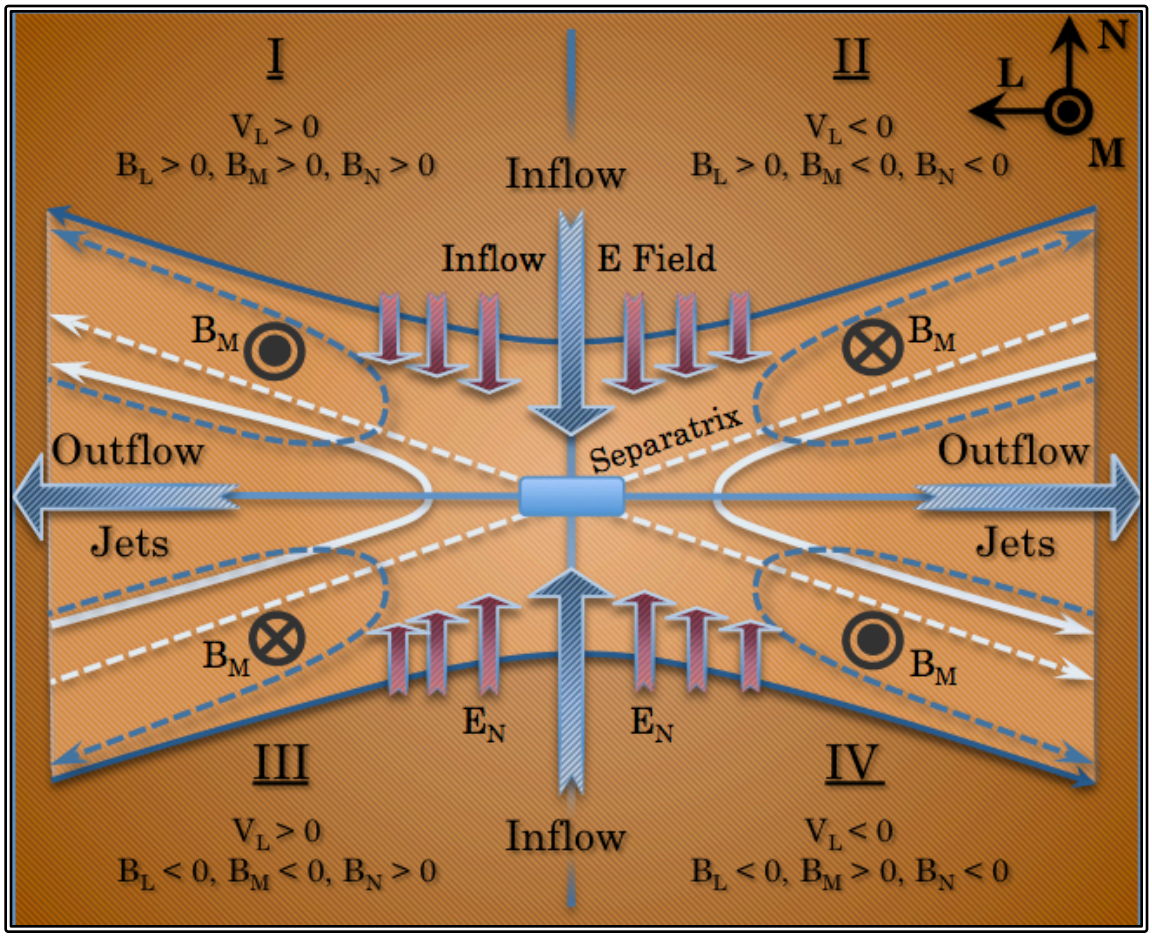

Figure 6: Greater detail of the reconnection region showing the electric field structure, the Hall (B_M) magnetic fields and the *LMN* boundary normal coordinate system. Figure adapted from *Paschmann et al.*, [2008].

The reconnection region, as depicted in Figure 6, is highly structured. The total structure can be divided into two main regions: the inflow and outflow regions. In the former, magnetic fields and plasma drift towards the boundary layer, and in the latter, magnetic fields and plasma are accelerated away from the X-line. The regions between the areas of inflow and outflow are called the separatrix and diffusion regions. Figure 7 gives the names and locations of the various regions within the reconnection structure.

The definition of the separatrix region used here is borrowed from *Lindstedt et al.,* [2009] (subsequently making it borrowed from *Gosling et al.,* [1990]). In the strictest sense, this definition of the separatrix region may not exactly define the region where the shocks form (the physical definition of the separatrix region). It is

chosen due to the difficulty of accurately locating the actual boundaries of a fluid shock structure experimentally.

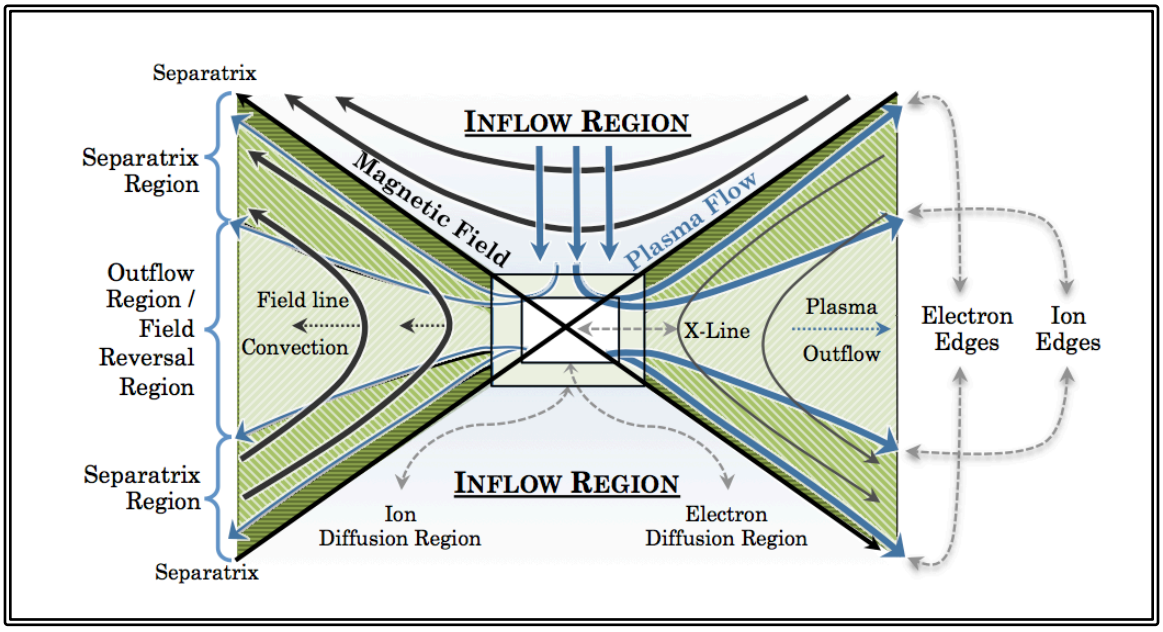

Figure 7: The structures and boundaries within the reconnection region. To the left, magnetic fields structures are emphasized. To the right, plasma flows and boundaries are emphasized. Figure adapted from *Lindstedt et al.,* [2009].

Located within the boundary between the inflow and outflow regions is a series of slow-mode shocks that originate in the diffusion regions and extend into the separatrix regions (*Petschek,* [1964]). Electric field structures within the shocks redirect plasma from the inflow to outflow regions (*Vaivads et al.*, [2006]). The properties of the diffusion regions and separatrix regions may vary according to the plasma conditions on either side of the current sheet boundary, and asymmetry in plasma conditions may result in asymmetries in the structure of the shocks and separatrices (*Lin and Lee*, [1994]). This is typically the case for reconnection at the magnetopause (*Levy et al.,* [1964]). Given plasma densities typical of magnetospheric reconnection, collisions between particles are not expected (*Sonnerup*, [1979]). With this in mind, shock structures that form should be purely fluid in nature and the reconnection mechanics should be described by Hall collisionless reconnection (*Sonnerup,* [1979], *Vaivads et al.*, [2006]).

Within the separatrix and diffusion regions heating and acceleration of plasmas occurs. Here ions are demagnetized from the inflow magnetic fields and magnetized to the outflow magnetic fields. Observations have been made of demagnetized ions within the separatrix region (*Khotyaintsev et al.*, [2006]), where the term demagnetized refers to the breakdown of the "frozen-in condition" (i.e. $\vec{E} + \vec{v_i} \times \vec{B} \neq 0$ within the separatrix region). Magnetization of the plasma from the inflow to the outflow magnetic fields occurs on various scales. The scale for demagnetization and heating of a species varies roughly scales with the inertial length of the particle, i.e. the scale that the demagnetization of electrons occurs on is much smaller than that of the protons. These scales have been established experimentally and via simulation.

As of yet, there has been no such study where the scale size of O^+ has been established. The existence of an O^+ scale would necessitate the full coupling (magnetization) of O^+ to the reconnection inflow/outflow fields. Due to the relatively small nature of the boundaries and structures where this coupling occurs, finite gyroradius effects may play a large role in limiting heavy ions from coupling to the reconnection region (*Mozer et al.,* [2002]). Despite this, observations have been made of accelerated heavy ions (specifically O^+) with velocities consistent with acceleration from heavy Alfvén waves originating from the separatrix/diffusion regions (*Chaston et al.*, [2005]) for one encounter with reconnection. This is far from rigorous though; this study will show via multiple case studies that O^+ is not limited by its large scale size during participation in reconnection physics.

In the following sections the structure of the reconnection region will be discussed in terms of the structures and dynamics of the reconnection magnetic fields and the particle flows (with specific focus on ion dynamics). In the section immediately following this, a new coordinate system will be introduced in order to better describe the reconnection geometry.

3.6.1. The *LMN* Boundary Normal Coordinate System

(*Russell and Elphic,* [1979]). Note that the various components of the fields in Figure 5 are defined in the coordinate system with axes *L*, *M* and *N*, the directions of

which are defined in the top right of the figure. This so-called *LMN* system is comprised of coordinate axes which are normal (*N*) and within the plane (*L, M*) of the magnetopause current layer. *L* is the direction tangent to the reconnecting field lines, *M* is the direction of the current flow in the boundary layer and *N* is the direction normal to the plane of the current layer. This system is the eigensystem of the magnetic fields of a discontinuity and is ideal for describing the geometry of the reconnection region.

3.6.2. Structure of the Magnetic Field

Though the normal component of the magnetic field in the reconnection region is typically the weakest (*Mozer and Retino*, [2007]), the observation of a non-zero B_N in a boundary region is a powerful tool in identifying a reconnection event. It is inherent to the structure of a rotational discontinuity (such as the reconnection region) and serves as a link between the fields and plasmas on either side of the boundary. A non-zero B_N is a necessary feature of the reconnection region. The condition that the magnetopause is an open boundary is what allows for plasma to actively diffuse across it (*Kivelson and Russell*, "Intro. to Space Phys.": The Magnetopause, Magnetotail and Mag. Reconnection). The normal is also the direction of magnetic flux into the reconnection region.

Assuming fully antiparallel reconnection, the *L* direction is normal to the magnetic field and points in the direction of curvature of the bent field lines. As mentioned previously, the bent nature of the field lines causes them to convect; the convective motion takes place in the *L* direction. The dynamics of the reconnection magnetic field in the *L* and *N* directions are shown in Figure 6. Magnetic field lines convect toward the reconnection along *N*, reconnect with one another, then convect away along *L*.

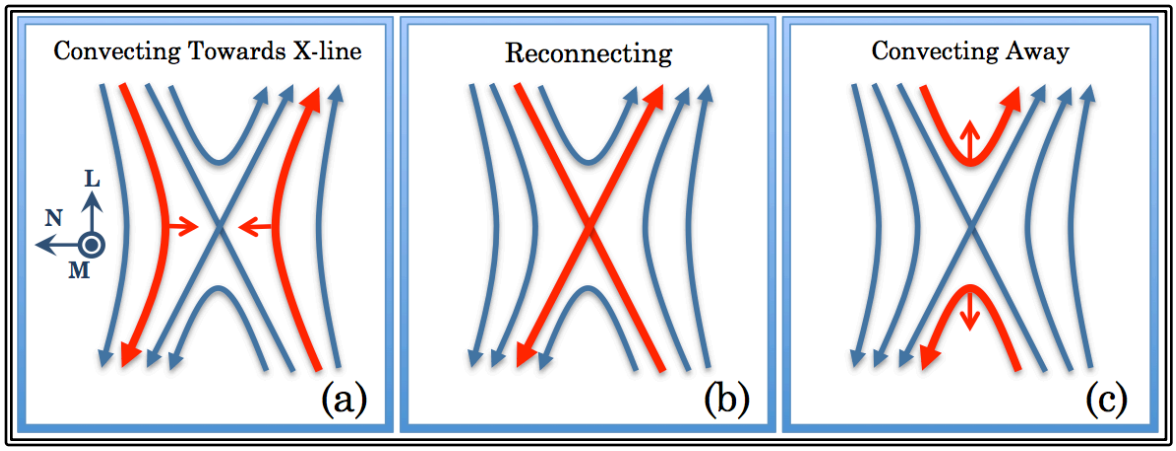

Figure 8: The dynamics of the Reconnection Magnetic Field in the *L-N* plane. The Hall B_M field is not included here. Field lines in panel (a) are called the inflow magnetic field lines. Those in panel (b) are the separatrices. Those in (c) are the reconnection/outflow magnetic field lines.

In steady state reconnection the out-of-plane magnetic field component is not particularly dynamical. It is generated by the current of inflowing and outflowing plasmas. The structure of the B_M field tends to be quadrapole, changing signs in each for the four quadrants shown in Figure 5 according the changes in direction of the current. The existence of the quadrapolar structure of B_M is indicative that collisionless Hall reconnection is taking place, and that non-zero Hall electric fields exist within the separatrix/diffusion regions (*Sonnerup*, [1979], *Vaivads et al.,* [2004]).

If asymmetries evolve in the structure of the region, some of these dynamics may appear skewed in terms of the *LMN* system. The existence of a so-called guide field is one possible feature of the reconnection region which adds asymmetries. Guide fields are generated when the reconnecting fields are not fully antiparallel, meaning component reconnection is occurring. Guide fields alter the behavior of the B_M or Hall component of the magnetic field. The presence of a guide field can be observed as an offset in the quadrapolar signature of the B_M field (*Lindstedt et al.*, [2009]). The effects of a guide field may also be manifested in a reduction to the reconnection rate (*Hesse and Birn,* [2004], *Fuselier et al.,* [2011]), and may alter the plasma flow geometry (*Fuselier et al.,* [2011]).

Each of these signatures discussed were used to aid in the identification of magnetopause reconnection events used in this study. The signs of B_L, B_M and B_N in each quadrant of the reconnection are listed in each of the four corners of Figure 5. This field geometry was used in this study to locate where the spacecraft was taking measurements when passing through a reconnection site. The location of the sign change of B_M however may be altered in the presence of a guide field (*Fuselier et al.,* [2011]). Depending on the strength of the guide field, a sign change of B_M may never occur (*Lindstedt et al*., [2009]).

3.6.3. Structure and Dynamics of Reconnection Plasma Flows

Inflowing plasma convects with the inflow magnetic fields into the separatrix/diffusion regions. Within the small diffusion layer the ions are demagnetized from the inflow magnetic fields and then magnetized to the outflow magnetic fields. Plasma in the outflow region convects with the magnetic fields. If the ions are entirely magnetized at both the inflow and outflow stages, their convective dynamics will roughly follow those shown in Figure 8. Convection typically drives the plasma along the direction perpendicular to the magnetic field. The plasma also inherits parallel, field-aligned motion from the electric field structure within the slow-mode shock (*Kivelson and Russell*, "Intro. to Space Phys.": The Magnetopause, Magnetotail, and Mag. Reconnection).

The total resulting plasma flow should be propagating at the local Alfvén velocity when taken in the inertial reference frame where the electric field is zero (the deHoffmann-Teller or dHT reference frame) (*Sonnerup et al.,* [1987]). The Alfvén velocity is best described as the speed at which disturbances to the magnetic field propagate through a plasma which is frozen-in to that field. The Alfvén velocity ($\vec{v}_A$) is given by Equation (2), $\vec{B}$ is the magnetic field vector, μ_0 is the permeability of free space ($4\pi\times10^{-7}\ \frac{\mathrm{V\cdot s}}{\mathrm{A\cdot m}}$) and ρ is the total mass density of the plasma (i.e. $\rho = n_1m_1 + n_2m_2 + \ldots n_km_k$ for a plasma with k distinct constituents). Here the effects of pressure anisotropy have been ignored.

$$\vec{v}_A = \frac{\vec{B}}{\sqrt{\mu_0\rho}} \tag{2}$$

Note that the Alfvén velocity is inversely dependent on the square root of the plasma mass density. One of the reasons O^+ might have a large effect on reconnection dynamics is that if O^+ is magnetized within the reconnection region it could have a large effect on the local Alfvén velocity. The identification of plasma flows that are Alfvénic in the dHT frame, e.g. those that obey the so-called Walén relation for a rotational discontinuity, will aid in the identification of reconnection events for this study. This will be discussed in *Section* 5.4. Identifying .

The combination of field aligned and non field aligned motions (generated by electric field acceleration and magnetic field convection respectively) generates separate 'edges' which bound the area of the outflow region accessible to the ions and the electrons (*Gosling et al.,* [1990]). The ion and electron edges are shown in Figures 5 and 7. Their observation will be used to help deduce the location of the microscale boundaries within the reconnection region.

3.6. The Reconnection Rate

The reconnection rate is described in *Borovsky et al.,* [2008] as "the amount of magnetic flux reconnecting per unit time, per unit length of the reconnection region". Roughly speaking, it describes the rate of transfer of magnetic field lines across the boundary (*Fuselier et al.,* [2005]). As a proxy for this quantity, the velocity of plasma inflow can be used to estimate the rate of reconnection. This is typically normalized to a dimensionless quantity by taking the ratio of the inflow speed with the outflow speed. Using the properties of the inflow and outflow speeds deduced in the previous section, the normalized rate of reconnection can be described by Equation (3) where R_{NORM} is the normalized rate of reconnection, v_{in} is the inflow speed, which is taken to be in the *N* direction, and v_{out} is the outflow speed, which, by the nature of reconnection, will be Alfvénic.

$$R_{NORM} = \frac{v_{in}}{v_{out}} = \frac{v_N}{v_A} \tag{3}$$

The rate of reconnection is also talked about in terms of the product of the normalized rate with the Alfvén speed (i.e. $R_{NORM} * v_A$). Typical given values for the

rate of fast reconnection are around $\sim 0.1 v_A$.[1] For slow reconnection this number can decrease by a factor of 10 or more (*Fuselier et al.,* [2011]). The reconnection rate is dependent on the plasma properties and the alignment and strengths of the two reconnecting magnetic fields.

Using mass flux conservation arguments its also convenient to link the rate of reconnection with the structure and geometry of the magnetic fields. Using arguments based on the geometry of the diffusion region and mass flux conservation, one can deduce the relation for the rate of reconnection given in Equation (4), where B_N and B_L are the magnetic field strengths in the N and L directions[2].

$$R = \frac{B_N}{B_L} * v_A \tag{4}$$

3.8. Summary of Theory / Restatement of Thesis

Energetic O^+ is commonly found within the magnetosphere. It originates in the ionosphere and can come to populate the inner magnetosphere by two primary means of transport. The activity of one such transport path is heightened drastically during times of geomagnetic activity, resulting in the amount of O^+ within the magnetosphere having a large amount of variability. Since O^+ is a much heavier ion than H^+ or He^+, the plasma mass density within the magnetosphere reflects this variability. O^+ may play a large role in influencing the parameters of reconnection due to its influence on the mass density and thus the local plasma Alfvén speed.

The simple fluid picture has O^+ decreasing the Alfvén speed and subsequently decreasing the reconnection rate. Using arguments which link the reconnection rate with the structure of the magnetic fields, O^+ may also influence the structure of the reconnection region. However, O^+ participation in reconnection is not guaranteed, as is the case with the simple fluid picture. This is due to the purely kinetic effects generated by the gyroradius of O^+ being of comparable size to

[1] Many studies, for instance *Vaivads et al.,* PRL, [2004] and *Mozer and Retino*, JGR, [2007]
[2] The relation between the structure of the diffusion region and the rate of reconnection has been used since the deduction of the Sweet-Parker and Petschek models. This specific variation is specific to the Petschek model and subsequently the model for collisionless Hall reconnection.

the reconnection region. If O^+ is unable to couple to the reconnection magnetic fields it may have no effect on the Alfvén speed or on the reconnection dynamics and structure.

In this study we wish to deduce the role of O^+ in magnetopause reconnection. By observing O^+ participating in reconnection related dynamics we can establish that O^+ is not limited by finite gyroradius effects from coupling to the reconnection magnetic fields. Next, we will establish the degree to which O^+ is magnetized within the reconnection region to deduce the degree to which it participates in the physics. If O^+ is at least partially magnetized within the reconnection region, we seek to establish the effects the O^+ content has on determining parameters such as the reconnection rate and the reconnection structure. Since there are many unknowns that may influence this (i.e. the existence of a guide field generated by component reconnection) this deduction can only be made in a detailed comparative statistical study. The study presented here can be considered the necessary precursor to such a large-scale study.

4. Existing Literature on Heavy Ions in Reconnection

4.2. Existing Experimental Studies

In brief, here are some relevant studies many of which have been mentioned previously. *Kistler et al.,* [2005], *Wygant et al*., [2005], *Zong et al*., [2001] and *Kasahara et al*., [2008] all reported observations of encounters with high energy O^+ outside the magnetopause boundary, concluding that reconnection was the likely source for its escape from the magnetosphere. *Marcucci et al.,* [2004] made similar observations but concluded the O^+ had escaped due to finite gyroradius effects. *Bourham et al.,* [2005] showed that O^+ is the dominant species in determining the plasma mass density at the magnetospheric side of the dusk magnetopause ~30% of the time. This O^+ dominance occurred at the dawn side, but less frequently. In an event previously studied by *Phan et al.,* [2003], *Chaston et al.,* [2005] reported observations of energetic O^+ with kinetic signatures indicative that it had been accelerated by heavy Alfvén waves originating in the separatrix region. *Phan et al.,* [2004] reported observations of energetic O^+ near an X-line in the high-latitude flank magnetopause. Over a 2-hour interval where continuous reconnection was observed, energetic O^+ was found in every jet.

4.3. Simulation / Theory

Hesse and Birn, [2004] modeled a three-species plasma in symmetric reconnection in a fully kinetic simulation. They found self-consistent acceleration of the O^+ generated by the Hall electric fields, but they found no effect of the O^+ on the reconnection rate. The authors note that O^+ was demagnetized within the reconnection region, a conclusion which may have been limited in some sense by the small box size of their simulations. *Shay and Swisdak*, [2004] modeled a three-fluid plasma, where the third fluid had a variable mass density. They observe the development of the various scales that develop within the microscale boundaries within the reconnection region. They deduce a net decrease of the reconnection rate when the variable mass density of the third fluid was increased. Fluid studies are

limited however, as they cannot address the heavy ion finite gyroradius effect as it is purely kinetic in nature. *Cassak and Shay,* [2007], determine the scaling laws for the reconnection rate, outflow speed and outflow density for asymmetric and antiparallel reconnection. *Cassak and Shay*, [2008] extends this analysis under the model of Hall collisionless reconnection. They found no dependence of the normalized rate of reconnection or outflow parameters based on asymmetries in the field or plasma conditions across the boundary. Since heavy ions affect the local Alfvén speed however, they did expect their presence to manifest itself as a net reduction in the un-normalized rate of reconnection. *Karimabadi et al.,* [2011] used a large-scale, fully kinetic particle simulation to study the effects of O^+ in reconnection. They found the effect of O^+ was to reduce the rate of energy conversion and broaden the quadrapolar structure of the Hall magnetic field. The effect of large-scale upwellings of plasmaspheric O^+ is observed by *Borovsky et al.,* [2008]. The effect of this upwelling of cold, heavy ions on reconnection, the so-called "plasmasphere effect", was observed to generate mass-loading at the reconnection region. This resulted in an increase in the Alfvén speed, decreasing the rate of reconnection by a factor of 2. As mentioned previously, this cold plasma will be ignored to the difficulty in detecting it experimentally with classic ion instrumentation.

4.4. Contributions of This Study to Current Understanding

In summary: while many experimental studies have established the presence of O^+ in/near the magnetopause reconnection region, and many more suggest it may be participating in acceleration, there has been no satisfactory analysis determining the level of O^+ involvement in reconnection experimentally. Simulation-based studies seem to draw varying conclusions on the effects of heavy ions on reconnection dynamics. There is currently a need for an experimental study to provide observational support of existing theory.

5. Methodology

In this study, we will provide observational evidence for the magnetization of O^+ via detailed case studies. These case studies are performed in the following manor. We will first identify magnetopause reconnection events and boundaries within the reconnection region using particle kinetic and magnetic field signatures. We will show that within the boundaries of the reconnection region, O^+ follows the kinetic signatures predicted by current models of collisionless Hall reconnection. This will be shown by exploiting well-established analytic techniques. This study will conclude with a look to the future by examining the possible directions it may be expanded in.

5.1. Overview of the Cluster Mission

This study is made possible by the comprehensive dataset of *in-situ* measurements made by the Cluster satellites. Consisting of four, well-equipped spacecraft, the Cluster mission orbits the Earth in an elliptical, polar orbit. The spacecraft spin once per four seconds, allowing for the three-dimensional properties of the nearby plasma and fields to be deduced with at least a four second resolution. The spacecraft are also oriented in a tetrahedral formation with a variable separation relative to one another. This configuration allows for the changes in the plasma and field conditions to be examined on a variable, three-dimensional spatial scale. The Cluster mission has been operational for more than ten years. During this time the four satellites have observed a multitude of crossings of the magnetopause at a variety of latitudes and MLT. This large database of comprehensive measurements is the key to this study.

5.2. Capabilities of the Cluster Spacecraft

The four Cluster spacecraft are equipped with a host of twelve instruments capable of generating a detailed description of the nearby plasmas, fields and waves. Magnetic field measurements are supplied by the flux-gate magnetometer (FGM)

capable of sampling the 3D magnetic field taken in high time resolution (67 Hz) (*Balogh et al.,* [1997]). The 2D electric field is available via the electric field instrument (EFW) in high time resolution (450 Hz) within the plane of the spacecraft spin (*Gustafsson et al.,* [2001]). The 3D structure of the electric field is deduced using the assumption that $\vec{E} \cdot \vec{B} = 0$. In regimes of weak magnetic field structure (e.g. near fields in the diffusion region) this measurement is not available. EFW also provides the spacecraft potential at equivalently high time resolution. This product can be used to deduce the electron density at high time resolution (*Pederson et al.,* [2008]). Electron distributions are measured with the plasma electron and current experiment (PEACE) instrument (*Johnstone et al.,* [1997]). The resolution of the electron measurements vary according to the operational telemetry mode of the instrument. Electron distributions are available at up to 2 second resolution.

5.3. The Cluster CIS / CODIF Instrument

Ion measurements are made by the Cluster Ion Spectrometry (CIS) suite of instruments (*Reme et al.,* [2001]). CIS consists of two distinct ion detectors, the hot ion analyzer (HIA) and the ion composition and distribution function analyzer (CODIF). HIA is capable of measuring ions within the energy range 5-32000eV/e. It is of limited use to this study, as it does not discriminate between the various species of ions. Rather, it takes all ions to be protons. The HIA instrument is operational on spacecraft 1 and 3 and samples ion distributions a maximum of once per spacecraft spin (4s). The CODIF instrument is capable of resolving the distributions of various ion species within the energy range 40eV-40keV. Like HIA, distributions are available at a maximum rate of once per spin. This study will rely on the H^+ and O^+ distribution function measurements taken from the CODIF instrument. It is operational on spacecraft 1 until 2004, spacecraft 3 until 2009, and spacecraft 4 for the duration of the mission.

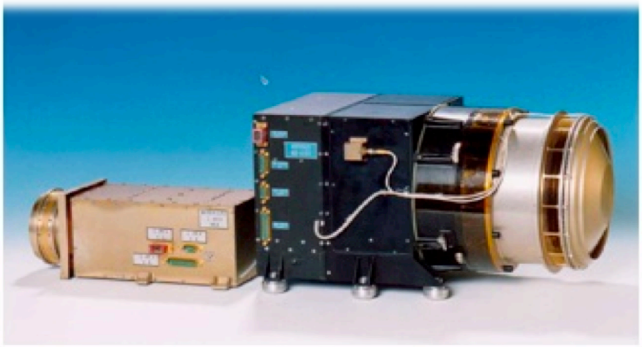

Figure 9: The CIS ion instruments. The CODIF ion composition instrument is on the right, HIA on the left. Image courtesy of UNH website.

CODIF is able to distinguish between the various species by exploiting a conjuncture of electrostatic and time-of-flight analysis techniques (*Mobius et al.,* [1998]). The electrostatic analyzer (ESA) of CODIF is able to discriminate ions based on their energy per charge ratio (E/q). The time-of-flight (TOF) analyzer is capable of deducing the velocity of the particle by measuring 'start' and 'stop' times as the particle traverses a known distance. The combination of these two measurements allows the induction of the mass per charge ratio, which is a unique quantity per each of the four species the instrument was designed to measure (H^+, He^+, He^{++} and O^+).

5.3.1. Saturation of Cluster-CODIF in High Count Rate Environments

In regions where plasma flux is very large (such as the magnetosheath) the TOF detectors on the CODIF instrument tend to become saturated. This occurs when the rate of particle flux through the instrument exceeds the maximum count-rate of the instrument. During these times the instrument is incapable of producing accurate estimations of the total number of particles passing through it, which results in a net underestimation of the particle density in the given TOF bin. However, the CODIF instrument has a second set of detectors (position detectors) which are capable of sampling the plasma at a much higher maximum count rate than the TOF detectors. Thus by monitoring the count rates of the two detector

systems it possible to: (a) identify times when the TOF detectors are saturated and (b) account for the 'missing' counts during such times.

This correction is called the 'high-rates correction'. It is done in two ways. One method is done by comparing the start/stop efficiency with the position detector count-rates. Ideally the start/stop efficiency should remain constant, but when count rates are large enough this value decreases. By fitting the curve of start/stop efficiencies (SEV/SFR) vs. position start (PF) count rates we can correct for any deviation from any non-linearity. The second method is done by comparing the TOF start (SF) with the position start (PF) measurements. Again, these two identical measurements should be made at count rates that scale with a 1:1 ratio. By comparing these two quantities we can deduce the level of saturation and account for missed particle counts. Figure 10 shows both count rate comparisons mentioned. Note that (a) the SEV/SFR drops off drastically at high PF count rates and that (b) the SF plateaus at high PF count rates. The functional fits of these distributions are shown superimposed upon the actual count rates data in black. The ideal detector responses (1:1 scaling for SF vs. PF and constant scaling of SEV/SFR vs. PF) are also shown in red.

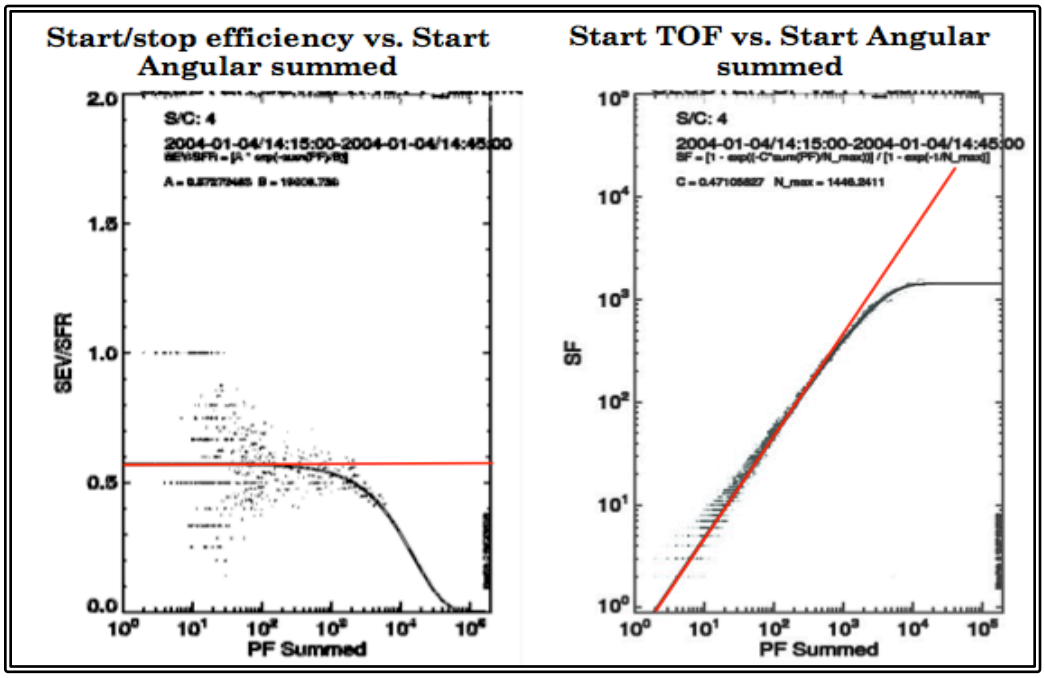

Figure 10: Comparisons of the TOF start/stop efficiency with position start count rates (left) and of TOF start with position start count rates (right) taken over a period when saturation of the TOF detector system is occurring.

5.3.2. Cross-Calibration Results of the High Rates Correction

Figure 11 show CODIF density measurements before and after the high-rates correction is applied. Density measurements from HIA are shown in blue and the deduced density from the WHISPER wave instrument is shown in red. These measurements are used to cross-calibrate the instrument to confirm the accuracy of the high-rates correction. Note that in Figure 11, during each encounter with the high-flux, low energy magnetosheath plasma, the CODIF-measured density (black) is much lower that of the other two instruments. Note also that the HIA instrument is underestimating the ion densities inside the magnetosphere. This is a known problem with the response of the instrument in the inner magnetosphere and it is not considered in this study as the HIA dataset has not been used.

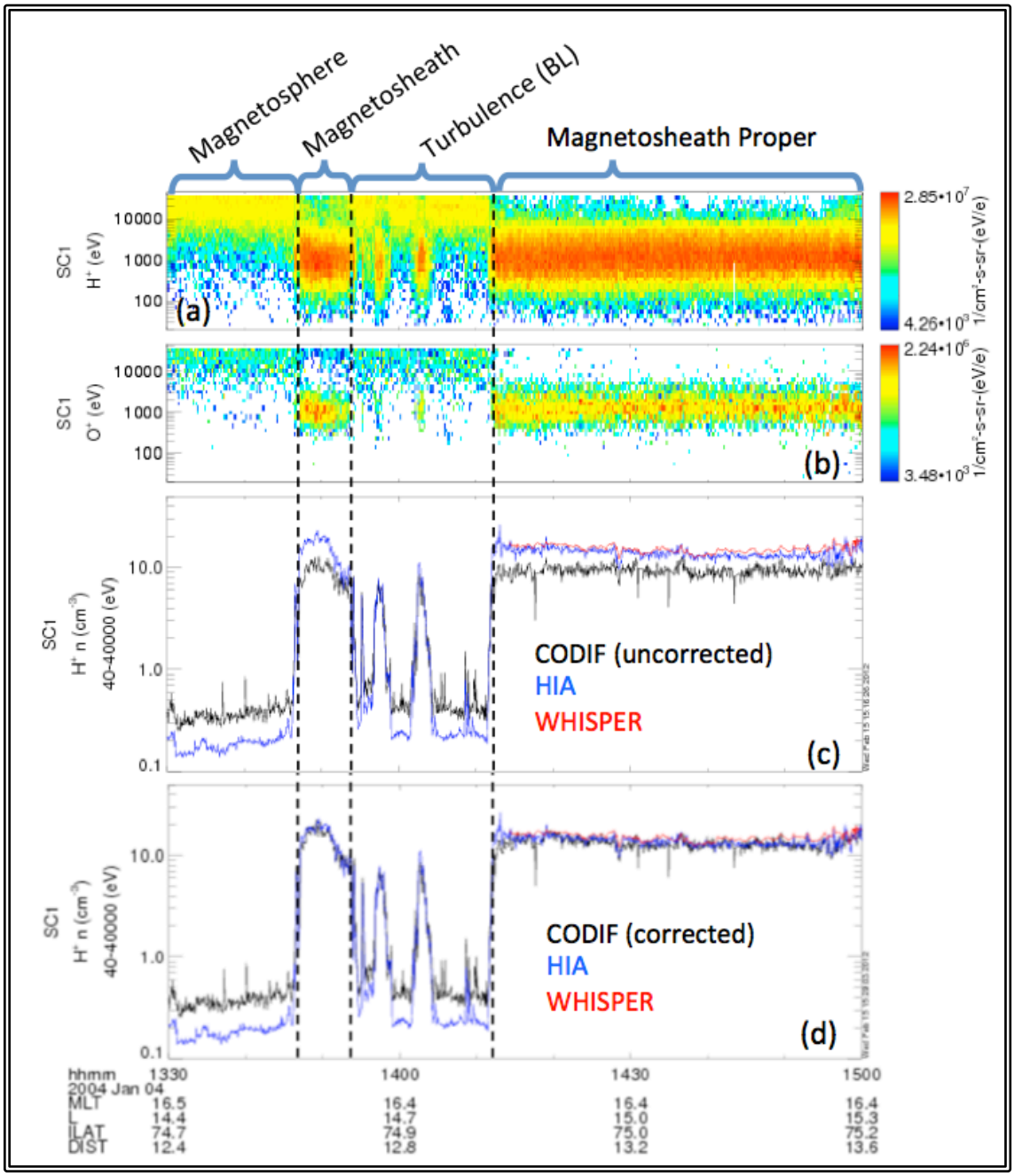

Figure 11: Cross-calibration of CODIF (black) with HIA (blue) and WHISPER (red) densities. In panel (c) CODIF measurements have not been corrected for saturation. In panel (d) CODIF measurements have been corrected using the fit deduced and shown in Figure 10.

During the entire interval shown in Figure 11 when WHISPER density data is available, the corrected CODIF H^+ and WHISPER deduced e^- densities are in almost perfect 1:1 agreement. This cross-calibration effort has given us confidence in the

CODIF H^+ measurements taken in the magnetosheath. This is an important and necessary first step to take before using this data for analysis.

5.3.3. Effects of Contamination of H^+ in the O^+ TOF Bins

Note that in Figure 11 there is a large amount of flux of low energy O^+ during times when Cluster is in the high-flux magnetosheath. Note also that this 'ghost-like spectrum' of O^+ mirrors the energy of the H^+ in this region. This is due to spillover of the tail of the H^+ distribution into the O^+ TOF bins. Though there may be real O^+ at these energies, they have been contaminated by the H^+ spillover. Thus this energy range of O^+ (roughly below ~5 keV) is not usable. However, since this study will show that O^+ streams in the reconnection region at roughly the same velocity as H^+ (meaning at 16x the energy) the effects of spillover can be ignored by limiting the energy range used in the calculation of the moments of the distribution function of O^+ to above ~5 keV. The difference between the full and energy-limited density moments of O^+ is demonstrated in Figure 12.

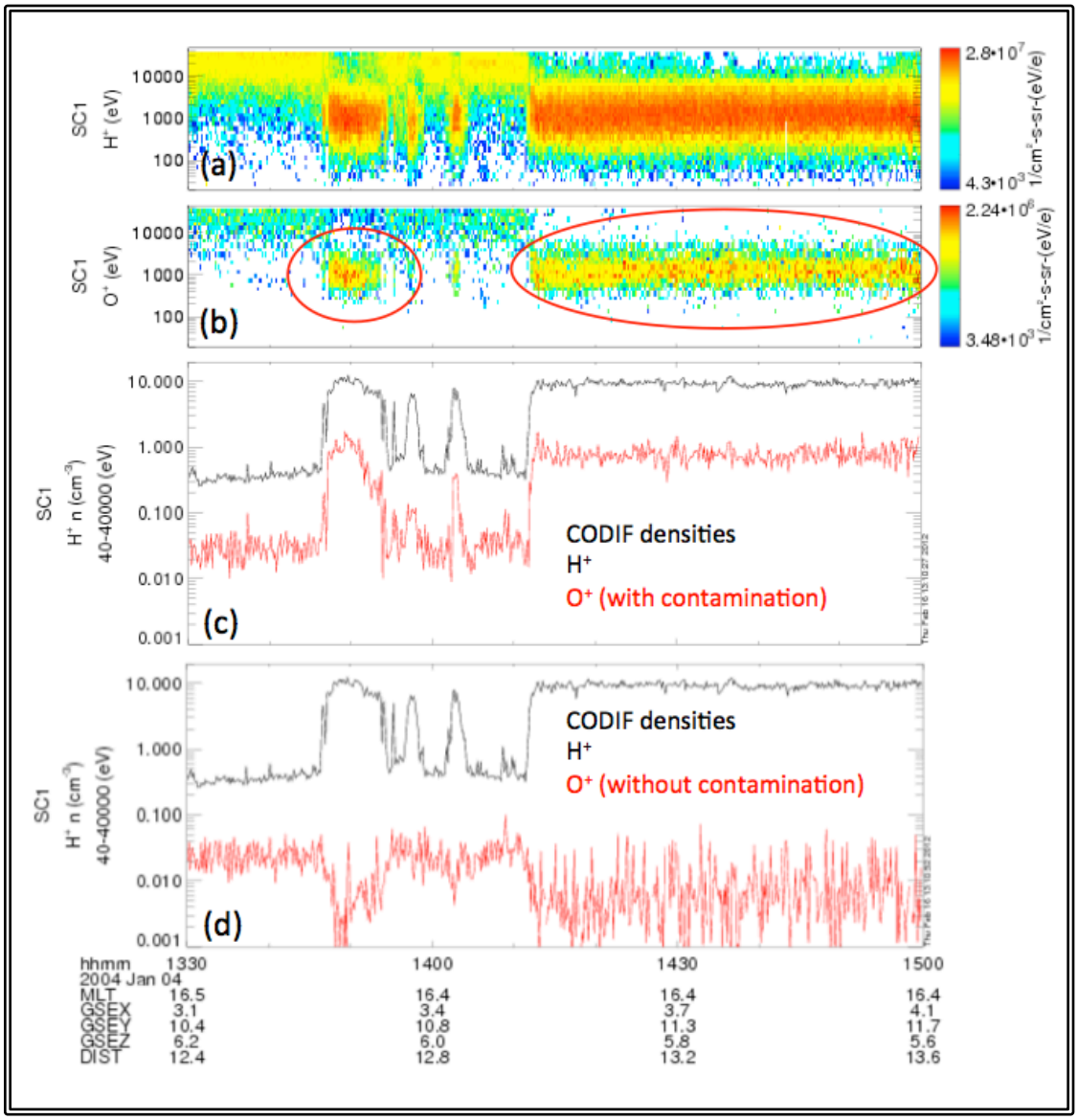

Figure 12: Example of H+ contamination of O+ TOF bins in high flux rate environments. In panel (b) the spectrum generated by contamination has been circled. Panel (c) shows O+ density moment calculated without energy limits. Panel (d) shows O+ density moment calculated using energies above ~5 keV.

The assumption that such a limited energy range of O+ is appropriate can be confirmed by close examination of the actual O+ distribution. Note that in Figure 12 the distribution of high-energy O+ shown in panel (b) drops off noticeably at energies well above 5 keV, where the effects H+ contamination become visible. This confirms that the lower bound of the O+ energy distribution is within the usable range of the instrument. The last such precaution we take is confirming that the

upper bound of the O^+ energy distribution is below 40 keV, the upper bound of the energy window of the instrument. In this study at least one event will be shown where such a cutoff below 40 keV is not observed.

The combination of self-consistent and cross-instrument calibration techniques have confirmed the accuracy of the CODIF dataset to a great degree of certainty. After ensuring that (a) the effects of contamination have been accounted for and (b) the effects of saturation have been accounted for we were able to establish confidence in the Cluster-CODIF dataset. In the following sections we perform analysis on this calibrated data with confidence in its accuracy.

5.4. Identifying Magnetopause Reconnection Events

The methodology employed in this study to identify Cluster encounters with magnetopause reconnection events goes as follows:

1) First we identify crossings of the magnetopause using magnetic field and plasma data. Such crossings are observed as a ~180° rotation of the magnetic field vector [1] coupled with a transition from magnetosheath to magnetospheric plasma, or vice-versa.
2) Next we identify which crossings within the pre-identified set display 'jet-like' spikes in the ion bulk velocity.
3) To confirm that these spikes in velocity are indeed reconnection jets, we check that they are Alfvénic in the frame of the convective electric field (the deHoffmann-Teller frame) using the Walén relation (*Sonnerup et al.,* [1987]).

The signatures of a magnetopause crossing (as observed by Cluster), the application of the Walén relation and the identification of the deHoffmann-Teller reference frame are all discussed in the following three sections.

[1] A ~180° rotation of the magnetic field across the magnetopause is only observed when the IMF is roughly antiparallel to the magnetospheric field. Since this is a condition necessary for reconnection, all events of interest will display this property.

5.4.1. Identifying Cluster Crossings of the Magnetopause

Identifying Cluster crossings of the magnetopause is not a rigorous process. As previously discussed, a crossing of the magnetopause is apparent in the plasma and field data. In the plasma data, it should appear as a crossing between the high-density, low-energy, anisotropic magnetosheath plasma to the low-density, low-energy, isotropic magnetospheric plasma, or vice-versa. Under conditions where the IMF is roughly antiparallel to the magnetospheric field, such a crossing would also have a roughly 180° rotation of the magnetic field. The identification of magnetopause crossings is also aided by the observation of O^+. Across the magnetopause, from magnetospheric to magnetosheath sides, the density of O^+ should drop off drastically. Some O^+ will most likely be observed close to the magnetopause, having crossed the boundary due to the finite gyroradius effect, but the density of O^+ should drop off rapidly with increasing distance away from the magnetopause. Figure 13 shows Cluster data from January 4th, 2004, when the Cluster spacecraft encountered multiple crossings of the duskside magnetopause. This event was studied previously by *Khotyaintsev et al.,* [2006] and again in *Lindstedt et al.,* [2009]. Eight of the prominent magnetopause crossings observed in this time interval are indicated with vertical lines. Solar wind and IMF data from the Ace spacecraft is also included (*McComas et al.,* [1998], *Smith et al.,* [1998]).

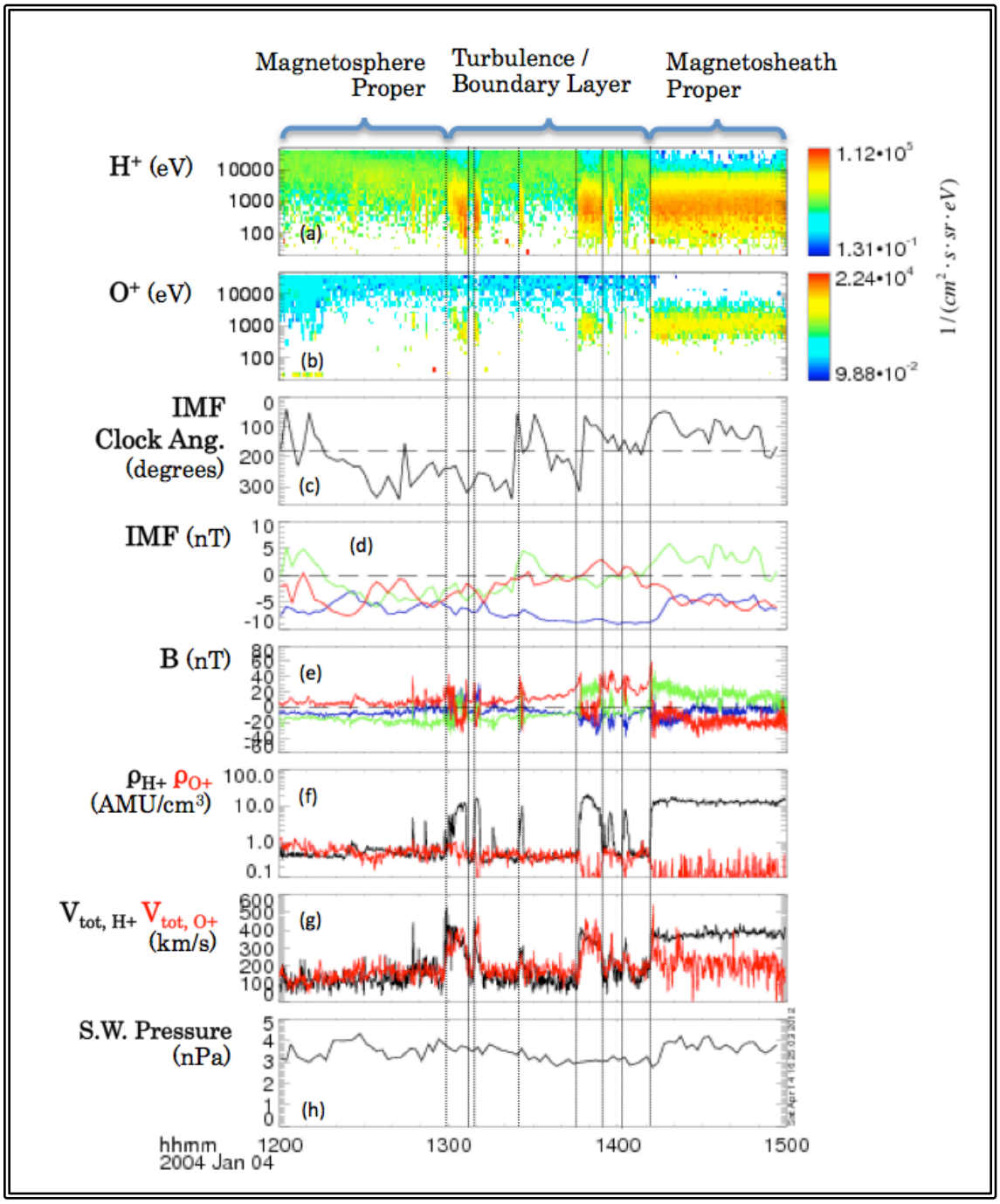

Figure 13: Data from Cluster 1 and ACE showing multiple crossings of the magnetopause, the most prominent of which are indicated with vertical lines. (a) H^+ differential flux from the CODIF instrument. (b) O^+ differential flux from CODIF. The effects of H^+ contamination are visible between ~5 keV - 500 eV. (c) The angle of the IMF in the Z-Y plane from ACE. (d) The three components of the IMF from ACE given in GSE. (e) The three components of the magnetic field from FGM. (f) The mass densities of H^+ and O^+ from CODIF. (g) The total bulk velocities of H^+ and O^+ from CODIF. (h) The solar wind dynamic pressure from ACE.

Note that each crossing of the magnetopause indicated corresponds to a rotation in the magnetic field, a drastic change in plasma density, a change from low-energy to high-energy H^+ (or vice versa). During many of the crossings, a large amount of high-energy O^+ was observed after Cluster crossed the magnetopause. This O^+ may have either leaked across the boundary due to the finite gyroradius effect or in reconnection related mixing.

Also note that many of these crossings correspond to spikes in the total bulk velocities of both H^+ and O^+, indicating that during many of these crossings the local magnetopause may be a rotational discontinuity. To confirm that such spikes in ion velocity observed in such an event are generated by reconnection of the magnetospheric field and IMF we use the Walén relation. In the section immediately following this the Walén relation will be defined. This will motivate the need to define the deHoffmann-Teller reference frame which will be done in the section following that.

5.4.2. The Walén Test for the Magnetopause as a Rotational Discontinuity

The Walén test is the primary analytic tool used in this study to identify rotational discontinuities and confirm that observed ion flows are reconnection outflows. The test was derived in *Sonnerup et al.,* [1981]. The relation is used to confirm that the plasma flows are Alfvénic in the deHoffmann-Teller (dHT) frame (the frame where the convective electric field is zero). The relation is given in Equation (5), where $\vec{v}$ is the measured velocity, $\vec{V}_{dHT}$ is the dHT velocity, ρ is the local plasma mass density, $\vec{B}$ is the local magnetic field vector, α is the pressure anisotropy factor and μ_0 is the permeability of free space.

$$\vec{v} + \vec{V}_{dHT} = \pm(1-\alpha)^{\frac{1}{2}} \frac{\vec{B}}{\sqrt{\mu_0 \rho}} = \vec{v}_A \qquad (5)$$

The sign of the right-hand-side of Equation (5) is determined by which side of the X-line the spacecraft encounters the jet. Note that the pressure anisotropy term, α, has been added to the Alfvén velocity as it is given in Equation (2). The anisotropy term is described in equation (6), where $P_{\parallel}$ and $P_{\perp}$ are the plasma pressures parallel and perpendicular to the magnetic field.

$$\alpha = (P_{\parallel} - P_{\perp})\frac{\mu_0}{2B^2} \quad (6)$$

In *Phan et al.,* [2001a, 2004b] he applies the Walén relation as it is given in *Sonnerup et al.,* [1987] using in-situ data from Wind and Cluster. From a single magnetosheath reference interval he computes the pressure anisotropy and mass density of the plasma, then uses these values to predict $\vec{v} + \vec{V}_{dHT}$ for multiple crossings of the reconnection region. He notes that this analysis is made possible because of the 'extreme steadiness of the IMF'. This is the methodology that this study employs, although multiple magnetosheath reference intervals are used to account for varying IMF conditions. The form of Equation (5) as it is given in *Phan et al.,* [2004] is given in equation (6) where the subscript '1' denotes values calculated from the magnetosheath reference interval.

$$\vec{v} + \vec{V}_{dHT} = \pm(1-\alpha)\frac{\vec{B}}{\sqrt{\mu_0\rho_1(1-\alpha_1)}} \quad (6)$$

5.4.3. Identifying the deHoffmann-Teller (dHT) Reference Frame

The dHT frame, as has been previously mentioned, is the inertial frame in which the convective electric field vanishes. More rigorously, it is the frame that satisfies Equation (7).

$$\vec{E}_C = \vec{v}\times\vec{B} = 0 \quad (7)$$

The existence of the dHT frame can be shown to be a necessary consequence of a finite B_N at the magnetopause. Given a finite B_N, the field lines on either side of the magnetopause will merge together, generating a non-zero value of $\partial\vec{B}/\partial t$. This value, according to Faraday's Law, is equivalent to $-\vec{E}_C$. In the dHT frame, both of these quantities are equivalent to zero, meaning all particle motion should be field aligned. It can be found by minimizing the residual electric field (denoted *D*) according to Equation (8) (*Sonnerup et al.,* [1987], *Khrabrov and Sonnerup*, "Analysis Methods for Multi-Spacecraft Data": deHoffmann-Teller Analysis).

$$D = \frac{1}{M}\sum_{m=1}^{M}|(v^{(m)} - V_{dHT}^{(m)})\times B^{(m)}|^2 \quad (8)$$

Here the superscript '*m*' denotes the m-th datapoint in a series of *M* total datapoints. The minimization requirement for *D* allows for a unique solution to the dHT frame

($\vec{V}_{dHT}$) to be deduced using least squares analysis (*Khrabrov and Sonnerup*, "Analysis Methods for Multi-Spacecraft Data": deHoffmann-Teller Analysis).

In this study, we will use three primary quantities as a measure of the accuracy of the dHT frame: the slope of the line fitting the measured vs. the deduced electric fields (i.e. $[\vec{E}_C = \vec{v}\times\vec{B}]$ vs. $[\vec{E}_{dHT} = \vec{V}_{dHT}\times\vec{B}]$), the correlation coefficient of the fit and the value of D/D_0, the definition of which is given in Equation (9).

$$D/D_0 = < |(\vec{v} - \vec{V}_{dHT})\times\vec{B}|^2 > / < |\vec{v}\times\vec{B}|^2 > \quad (9)$$

For a good dHT frame, the value of D/D_0 should be much smaller than one (in the ideal frame, D=0) (*Sonnerup et al.,* 1987).

5.5. Finding and Quality Checking the *LMN* Coordinate System

As stated previously in *Section* 3.6.1. The *LMN* Boundary Normal Coordinate System, the *LMN* boundary normal coordinate system is the eigensystem of the current layer boundary (*Russell and Elphic,* [1979]). Subsequently, the *LMN* system is also the eigensystem of the local magnetic field at the boundary. As discussed in *Sections* 3.6.2. Structure of the Magnetic Field, 3.6.3. Structure and Dynamics of Reconnection Plasma Flows and 3.6. The Reconnection Rate, deduction of the *LMN* coordinate system allows for a much more powerful description of the magnetic field and plasma dynamics and of the overall reconnection structure and rate. In the most rigorous sense, proper Walén analysis of the reconnection jets necessitates knowledge of the *LMN* coordinate system. This is because the location of the outflow region can be defined with a great deal of precision using the high resolution magnetic field data. In the LMN system, determination of the outflow region boundaries can be determined according to the signatures described in *Section* 3.6.2. Structure of the Magnetic Field.

Many methods for determining the *LMN* system with single and multiple spacecraft datasets exist in the literature. Two of the more commonly used techniques are minimum variance analysis (MVA) and timing analysis of the boundary motion; the former (MVA) requires one spacecraft, the latter (timing analysis) requires four closely-spaced spacecraft (*Sonnerup and Scheible*, "Analysis

Methods for Multi-Spacecraft Data": Minimum and Maximum Variance Analysis, *Schwartz*, "Analysis Methods for Multi-Spacecraft Data": Shock and Discontinuity Parameters, [2000]). This study will focus on MVA as the primary technique for deducing the *LMN* system.

MVA, in essence, is a spatially averaged eigenvalue problem. It can be shown that after rigorous mathematics (*Sonnerup and Scheible*, "Analysis Methods for Multi-Spacecraft Data": Minimum and Maximum Variance Analysis) that by defining the vector normal to the boundary as the direction in which the magnetic field varies least it follows that the *LMN* vectors can be solved for by minimizing the magnetic field variance, σ^2, as it is given in Equation (10). Here the magnetic field is shown to consist of a set of measurements with *M* total data points.

$$\sigma^2 = \frac{1}{M}\sum_{m=1}^{M} |(B^{(m)} - < \vec{B} >) \cdot \widehat{N}|^2 \tag{10}$$

Furthermore, when the constraint that $|\widehat{N}|^2 = 1$ is imposed on the minimization of σ^2, the vectors of the *LMN* system can be shown as the eigenvectors of the magnetic variance matrix, M^B (*Sonnerup and Scheible*, "Analysis Methods for Multi-Spacecraft Data": Minimum and Maximum Variance Analysis). The various components of M^B are given in Equation (11), where μ and υ run from 1 to 3 and represent the three components of the initial coordinate system. The eigenvector problem of M^B are given in Equation (12), where $\widehat{N}_\mu$ and $\widehat{N}_\nu$ are the projections of the normal vector onto initial coordinate axis μ and ν.

$$M^B_{\mu\nu} \equiv < B_\mu B_\nu > - < B_\mu >< B_\nu > \tag{11}$$

$$\sum_{\nu=1}^{3} M^B_{\mu\nu}\, n_\nu = \lambda n_\mu \tag{12}$$

Equation (12), since M^B is symmetric and real valued, allows for exactly three solutions where λ is real valued. The corresponding eigenvector set, $\{\hat{L}, \widehat{M}, \widehat{N}\}$, are all orthogonal by the same condition. As a set they represent the directions of the maximum, intermediate and minimum variance of the magnetic field, respectively (*Sonnerup and Scheible*, "Analysis Methods for Multi-Spacecraft Data": Minimum

and Maximum Variance Analysis). Since the value of λ represents the actual magnetic field variance, the $\hat{L}, \widehat{M}$ and $\widehat{N}$ vectors whose corresponding λ values are the largest, intermediate and smallest of the set.

Though MVA is sometimes thought of as a more error-prone approach to find *LMN* than timing analysis (*Schwartz,* "Analysis Methods for Multi-Spacecraft Data": Shock and Discontinuity Parameters [2000], *Fuselier et al.,* [2005]), we find that MVA, coupled with error analysis and multiple spacecraft cross-checking, is fairly accurate and certainly accurate enough for this study. Several techniques have been developed to estimate the error in MVA (*Kawano and Higuchi,* [1995]); we will use these arguments in a less-than-rigorous manor and rely more heavily on confirmation of the MVA system from multiple spacecraft.

One such proxy for the error of the MVA system is given by the separation of the three eigenvectors λ_L, λ_M, and λ_N. The limit in which any two eigenvalues approach the same value is the limit in which those two solutions become degenerate (i.e. if $\lambda_L=\lambda_N$ the eigenvector set would be degenerate in *LN* space and no meaningful description of the boundary normal would be attainable). Thus a good MVA coordinate system can be equated to one with large separation between the normal and coplanar eigenvalues, meaning $\lambda_M/\lambda_N >> 1$. Here λ_M is chosen over λ_L to define this ratio since, by definition, $\lambda_M \geq \lambda_L$. (*Sonnerup and Scheible*, "Analysis Methods for Multi-Spacecraft Data": Minimum and Maximum Variance Analysis).

Another condition we will use as a measure for a good MVA system is that the direction of the $\hat{L}, \widehat{M}$ and $\widehat{N}$ vectors should be insensitive to small changes in the time interval used (e.g. the span of data points used in the MVA is changed slightly). In the method employed in this study we manually vary the time interval wherein the MVA is performed. If any observably large rotation of the coordinate axes are observed then the MVA system is deemed unstable.

One more simple test for the accuracy of the MVA system can be done if multiple spacecraft are spaced close enough so that they encounter the same region of a boundary at roughly the same time. If this spacecraft geometry is available then

multiple spacecraft can be used for analysis and the MVA systems from the two can be compared. If the vectors are closely spaced, the accuracy of either system can be confirmed. If the two systems are close then the system with the highest eigenvalue ratio is chosen.

5.6. Methods for Determining the Rate of Reconnection

Several methods for determining the rate of reconnection have been proposed in the existing literature. Since these techniques are only relevant to the section of this study where we discuss future work, all these concepts will be discussed in brief. The first method has already been mentioned, it involves direct observation of the ratio of v_{in}/v_A (see Equation (3)). Since an accurate description of v_{in} requires the utmost certainty in the direction of the normal, this method is prone to error. The theory was described in detail in *Sonnerup et al.,* [1979] and carried out in *Phan et al.,* [2001] with varying success. Using various techniques for determining the boundary normal, *Phan et al.,* [2001] reported variations of the normalized reconnection rate between ~0.2 and ~0.01 for the same reconnection event. In this study, rather than use direct observations of the inflow and outflow speeds from multiple spacecraft, he uses $V_{dHT} \cdot \widehat{N}$ as the estimated inflow speed. This may have invited further error in his calculation of the reconnection rate.

A related argument involves describing the normalized reconnection rate as B_N/B_L. This methodology was used in *Vaivads et al.,* [2004] where he found a normalized reconnection rate of ~0.1. He was also able to confirm this calculated value by comparing with direct observations of the tangential and normal electric fields. Such observations are rare, and again, the calculation of the normal using conventional methods is prone to error. Using the appropriate methods for tracking error in the MVA system however, this method may prove viable. It is also possible however that this method may not be applicable for component reconnection, when the geometry of the reconnection region is skewed in the *LM* plane.

One last method is the 'multi spacecraft' technique described in *Fuselier et al.,* [2005]. Using simplifications of the geometry of the reconnection region, he argues that it is possible to link the distance between the spacecraft and the diffusion

region with the rate of reconnection via multiple observations of the local 'cut-off' velocity of ions within the reconnection region. He proposes that if multiple spacecraft were located in the outflow region at staggered distances away from the diffusion region they should observe a different local 'cut-off' ion velocity. This is due to the fact that ions below that certain velocity would not be able to access the same regions as higher energy ions under certain assumptions regarding the reconnection rate. This method requires a very particular spacecraft geometry relative to the diffusion region, but links the distance to the diffusion region to the reconnection rate. Both these values are notoriously difficult to find, so this may prove to be a very important experimental technique for determining both.

6. Results and Analysis

6.1. February 20, 2002

6.1.1. Event Overview

During February 20th, 2002, the four Cluster spacecraft encountered multiple crossings of the magnetopause boundary layer. The spacecraft were located tailward of the cusp in the plasma mantle / magnetosheath. The location of the spacecraft is shown in Figure 14. The magnetosphere in Figure 14 is estimated using the Tsyganeko 96 (T96) model (*Tsyganeko,* [1995]). The spacecraft separation was small (≤200km) and the CODIF instruments on spacecraft 1 and 4 were in 8s telemetry mode. The IMF B_z was mostly northward, though the strength was weak and variations of the sign of B_z were observed. Such a northward IMF is consistent with reconnection occurring tailward of the cusp along southward magnetospheric field lines. A strong IMF $+B_y$ was observed throughout the duration of the event. An estimate for the average IMF clock angle is <100° but this varied with sign of B_z. The strong B_y suggests component reconnection may have been occurring. Figure 15 shows a brief overview of the event. The geomagnetic activity during this time was low, as indicated by the DST index, which suggests that this was a non-storm time event. Moderately sized variations in the solar wind flow pressure were observed during the interval, indicating that these crossings of the magnetopause were most likely generated by fluctuations in the pressure balance relationship (see *Section* 3.2. The Magnetopause Boundary Layer). The moderate size of the solar wind pressure variations would be consistent with small variations in the magnetopause location. This would be consistent with Cluster staying within the boundary region between 13:00-14:00 UT.

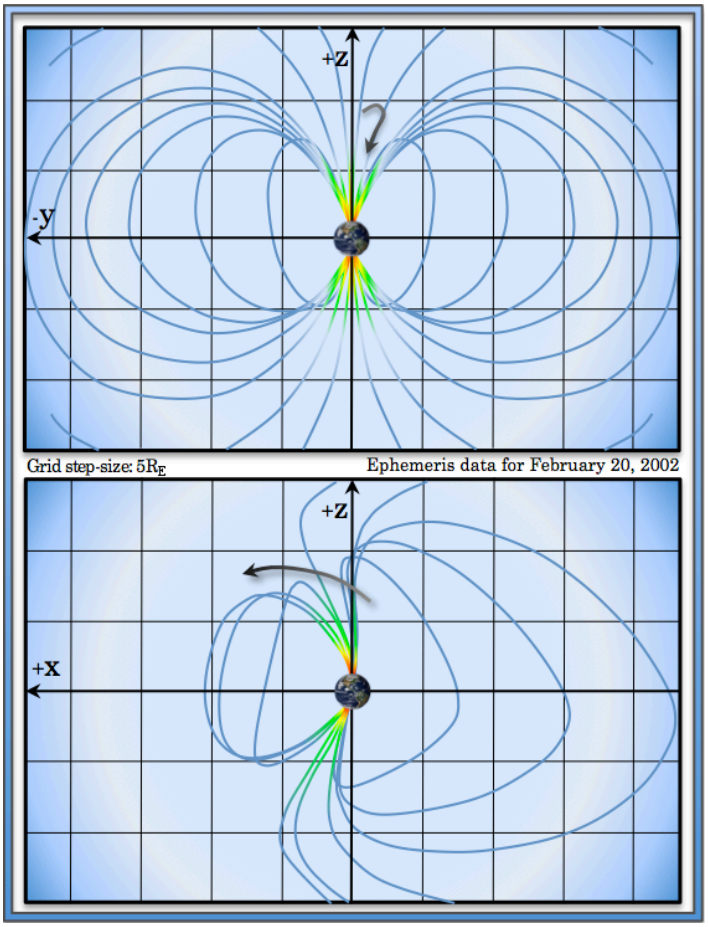

Figure 14: Cluster ephemeris data for 2002-02-20 13:00-15:00UT. Made with the help of the Orbit Visualizer Tool (http://ovt.irfu.se/download.jsp).

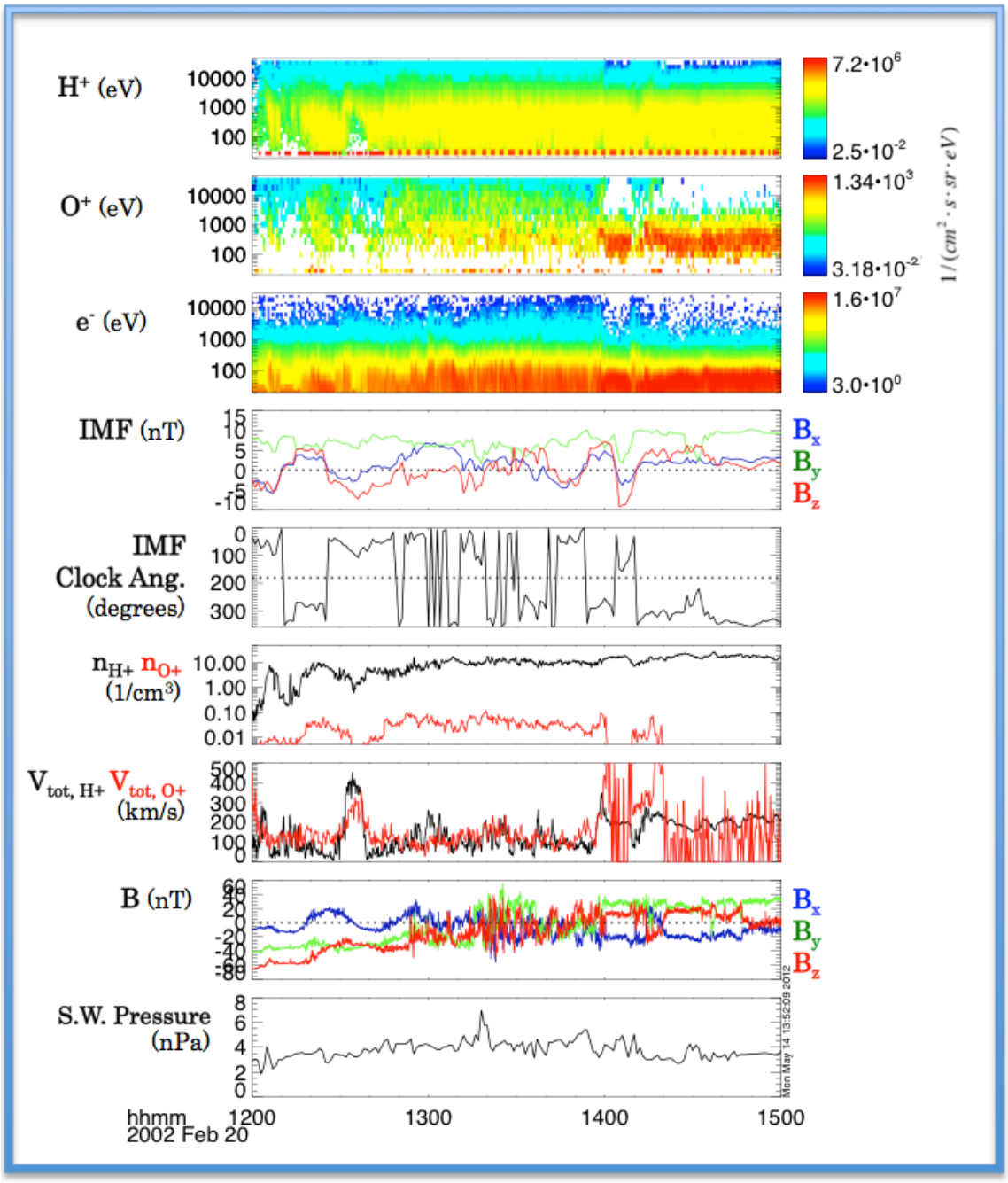

Figure 15: Overview of February 20, 2002 event with Cluster and ACE data.

Between 13:00 and 14:00 UT multiple rapid crossings of the magnetopause were observed. Cluster remained in a boundary region characterized by a mixture of sheath-like plasma and high-energy magnetospheric-like plasma. During this entire interval high-energy (>2 keV) O^+ was observed at a density of ~0.03 cm^{-3}. The density ratio of n_{H+}/n_{O+} was around 300. The mass density ratio of ρ_{H+}/ρ_{O+} was

around 20. *Vaivads et al.,* [2004] performed a case study of a magnetopause reconnection event within this interval. He observed continuous reconnection throughout the entire interval 13:00 – 14:00 UT. He reports a normalized reconnection rate of ~0.1 for the event studied using the method given in Equation (4). He also reported that the Cluster spacecraft were within a close vicinity to the diffusion region as made evident by the strength of the Hall electromagnetic field. The reconnection studied by *Vaivads et al.*, [2004], along with many other crossings within this interval, was too rapid for the CODIF instrument to sample a full 3-D distribution within the reconnection region making these events of limited use for this study.

Between 14:00 and 14:30 UT Cluster observed several full crossings of the magnetopause between the magnetosheath proper and the plasma mantle. Similar high-energy was observed on the magnetospheric side of the magnetopause. At the magnetopause boundary, accelerated O^+ (~4 keV) was observed. This O^+ population dropped off during times when Cluster was far from the magnetopause on the side of the magnetosheath. Finite gyroradius O^+ characterized by a bulk velocity with a ~90° pitch angle was observed close to the edge of the magnetopause on the magnetosheath side of the boundary.

6.1.2. Calibration of Cluster-CODIF

Calibrations for the effects of high count rate saturation were performed for the CODIF H^+ product as discussed in *Section* 5.3.1. Saturation of Cluster-CODIF in High Count Rate Environments. Though WHISPER density data was not available for this interval, a favorable comparison was found between CODIF H^+ and HIA H^+ densities post-calibration. Contamination of the CODIF O^+ product from H^+ spillover was visible between 100 eV and 2 keV. During encounters with accelerated H^+ at the magnetopause, the contamination is observed at higher energies, the upper bound of which was around 4 to 5 keV. The calculation of the moments of O^+ was performed using the limited energy distribution between 5 – 40 keV.

6.1.3. Qualitative Assessment of Jet

Around 13:59 UT Cluster CODIF observed a with a reconnection jet-like ion flow during a crossing of the magnetopause. The boundary movement was such that the Cluster spacecraft were present in the jet-like region for more than 1 minute (13:57:30 – 13:59:00 UT). Acceleration signatures in the H^+ and O^+ differential flux spectra were observed, as well as a factor of ~2 enhancement of the H^+ bulk velocity (as measured from the magnetosheath side of the encounter). In this time Cluster observed multiple rapid reversals in the magnetic field vector, alternating between a weakly southward oriented field (consistent with the expected magnetospheric field) and a northward magnetic field with a strong $+B_y$ component (consistent with the IMF field signature). Throughout the 2 minutes where these rapid fluctuations were observed the ion and electron differential fluxes stayed fairly uniform, suggesting that mixing of plasmas was taking place between the regimes of magnetospheric and magnetosheath magnetic fields. Figure 16 shows this in detail.

During this time within the jet-like ion flow region the total velocity of O^+ was slightly less than that of H^+. The velocity of O^+ perpendicular to the magnetic field closely matched that of H^+ for the same interval, which suggests in a qualitative sense that O^+ may have been involved in convective reconnection dynamics (see *Section* 3.6.3. Structure and Dynamics of Reconnection Plasma Flows). Were this to be true, O^+ would have to be frozen-in to the reconnection fields by necessity, meaning the finite gyroradius was not inhibiting the magnetization of O^+. More quantitative analysis is necessary to (a) prove the jet-like flow is propagating at the Alfvén speed taken in the dHT frame and (b) prove that O^+ is mirroring the dynamics of H^+ in the reconnection region. First we will determine the *LMN* coordinate system to deduce the location of the outflow / field reversal region. In this region the Walén test will be performed. (*Note that after this interval (13:59:30+ UT), the sporadic nature of the O^+ velocity was due low count rates and poor statistics*).

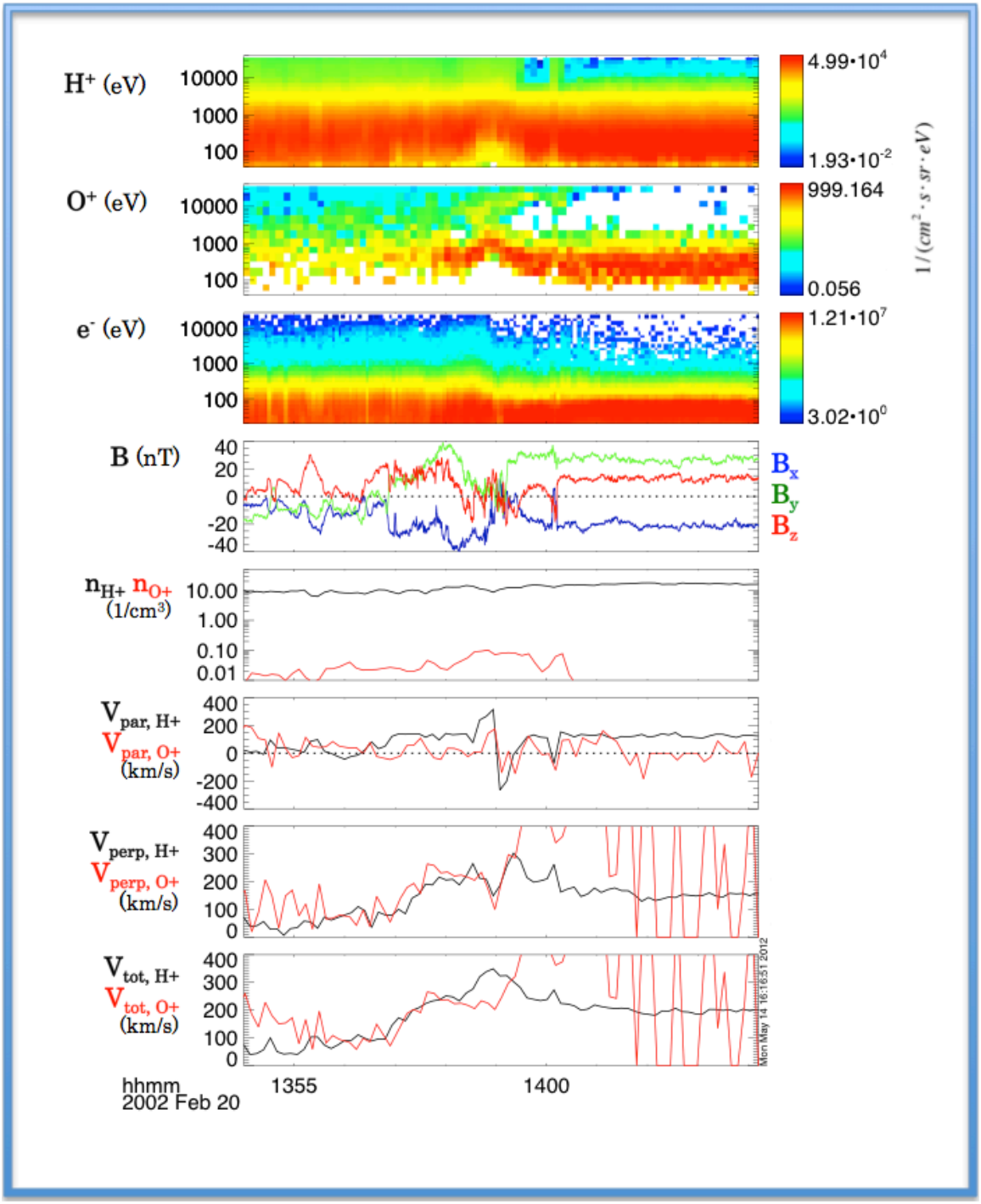

Figure 16: Long duration, turbulent encounter with the accelerated ion flow on Feb 20, 2002. Data here is from Cluster 1. Each of the four spacecraft observed almost identical field and particle signatures.

Analysis of the O^+ and H^+ distribution functions help to describe the ion dynamics from a different point of view than the moments calculations. Figure 17

shows the pitch angle distributions of O^+ and H^+ before the jet while Cluster was in the plasma mantle (frames (a) and (b)), during the time while Cluster was in the jet (frames (c) and (d)) and when Cluster was in the magnetosheath (frames (e) and (f)). Note that the top two panels show the two species as being roughly isotropic. During this time Cluster was on the magnetospheric side of the magnetopause. In panels (c) and (d) O^+ and H^+ have bulk velocities in roughly the same direction pointing towards the ($+V_{par}$, $+V_{perp}$) direction. H^+ contamination in the O^+ distribution is the red, high flux-density region bounded by 0 velocity and +50 km/s V_{par}, +50 km/s V_{perp}. In panel (e) the high energy H^+ population has dropped out, leaving a lower energy, lower temperature flow in roughly the same direction as the jet-like flow. In panel (f) the O^+ distribution is centered roughly around the 90° pitch angle line, indicating that this is most likely finite gyroradius O^+. Note that all panels shown in Figure 17 are an integration of multiple 4 second resolution distributions. Typical integration time was ~1 minute; the specific time of integration is indicated on the top of each panel.

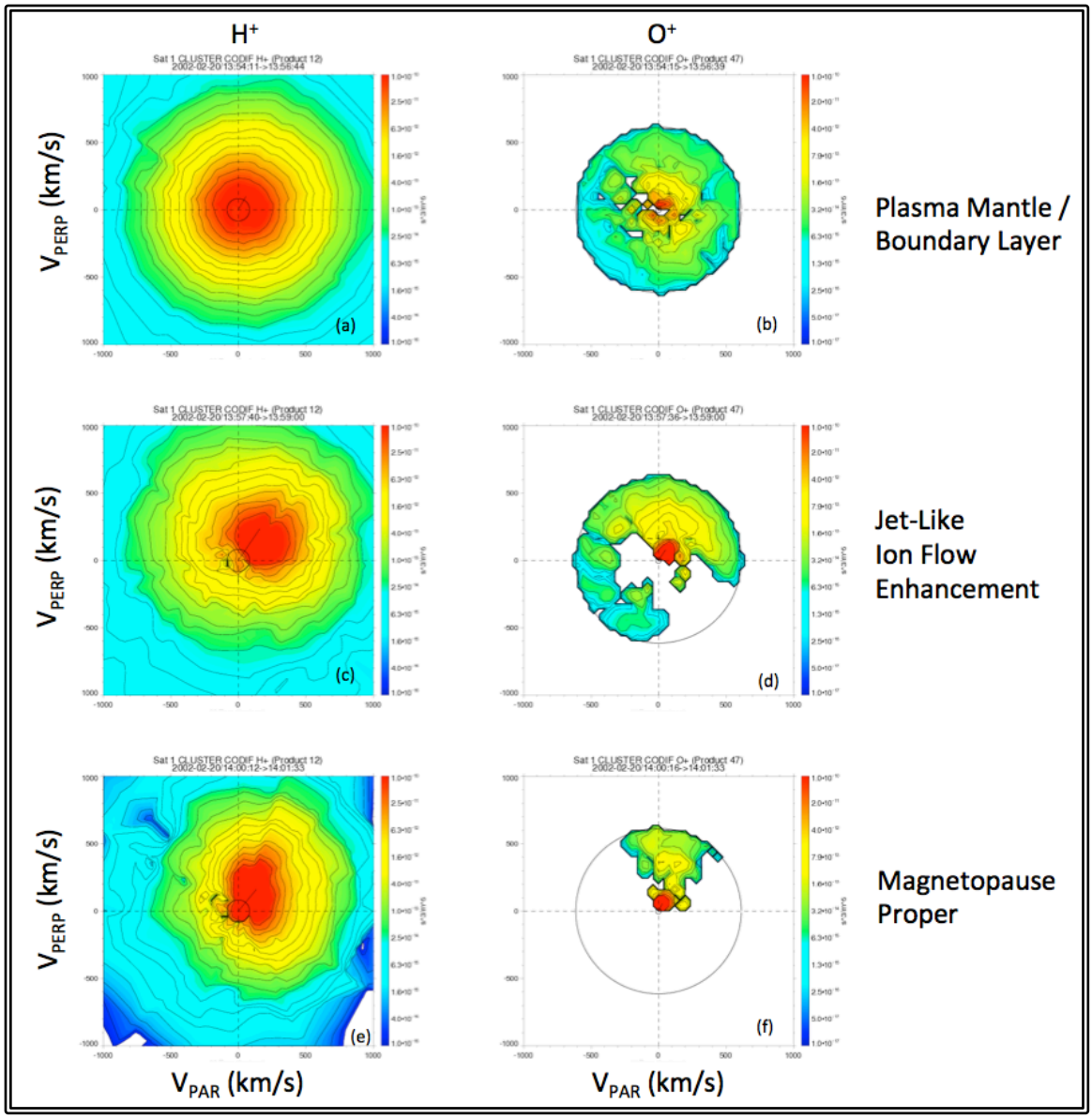

Figure 17: 'Before', 'during' and 'after' images of H^+ and O^+ distribution functions taken relative to the time of 2002-02-20 13:58 UT jet encounter.

6.1.3. Results from Minimum Variance Analysis

Minimum variance analysis was performed using magnetic field data from all four spacecraft as they encountered the magnetopause boundary within 1 second of one another. The time of the crossing was approximately 13:59:08 UT. Though multiple crossings of the current sheet were observed around this time, the MVA calculation for this crossing yielded the highest average eigenvalue ratio as well as the closest angular agreement between the eigenvectors of each of the four

spacecraft. Figure 18 shows a 3-D box plot where each of the *LMN* systems from each spacecraft are plotted in GSE. Here the *L* vector is shown in green, the *M* vector in blue and the normal vector in red. The various line styles represent the vectors from each of the four spacecraft; spacecraft 1 is the solid line, spacecraft 2 is the dotted line, spacecraft 3 is the dashed line and spacecraft 4 is the dashed-dotted line. Looking at the relative spacecraft location as shown in Figure 14, one can imagine that the normal to the magnetopause should lie roughly along the *+x* GSE axis with small *–z* and *+y* components. This is almost entirely confirmed in the plot shown below, though here a small *–y* component is observed in the normal.

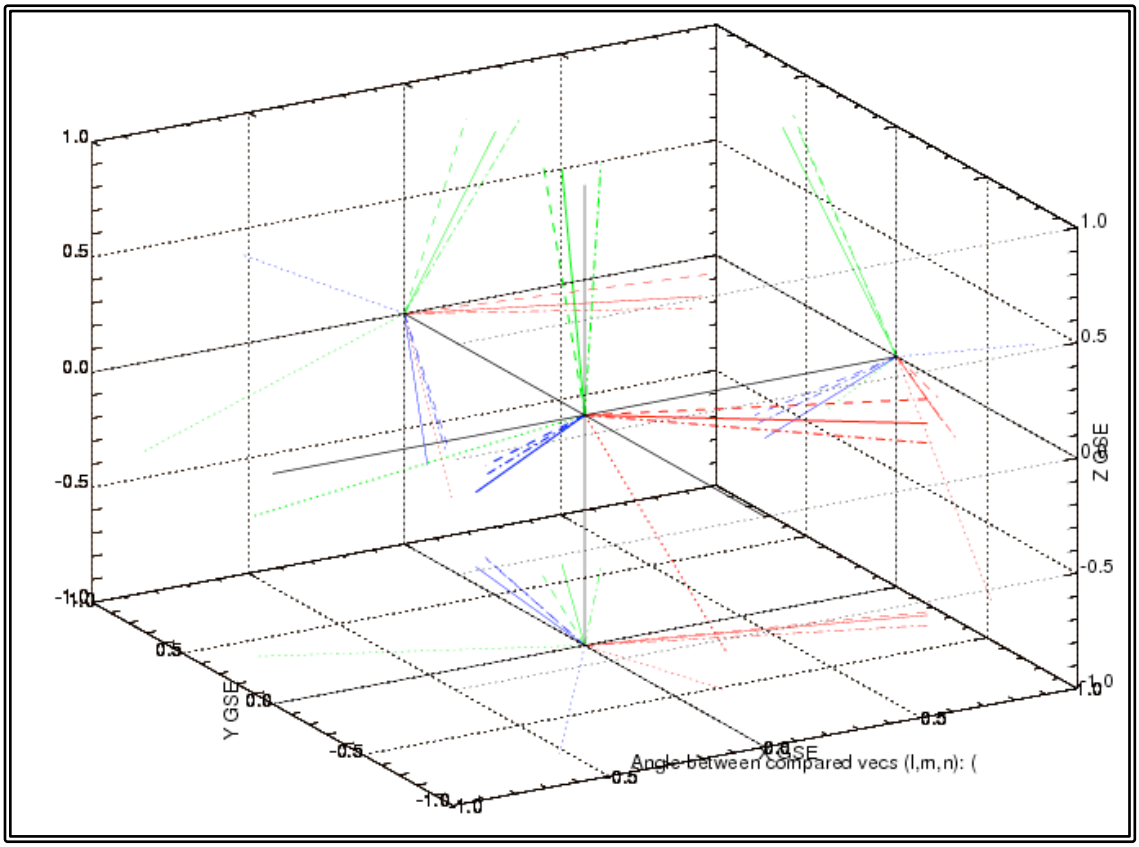

Figure 18: The *LMN* coordinate vectors calculated using magnetometer data from each of the four Cluster spacecraft during a current sheet crossing at 13:59:07 UT.

Tables 1 and 2 document the results from the MVA calculations on each spacecraft. Table 1 gives the MVA parameters of magnetic field information for each spacecraft. Table 2 gives comparisons between of the four spacecraft. In this

comparison, spacecraft 2 was the outlier of the four. Each of the three coordinate vectors for spacecraft 1 and 4 were in very close angular agreement (≤3°) and both observed a normal magnetic field of comparable strength. A noticeable but small angular separation is observed between the coordinates for spacecraft 3 and those for spacecraft 1 and 4. Though spacecraft 3 had the highest eigenvalue ratio and lowest standard deviation in the normal magnetic field vector, spacecraft 3 was at a greater distance from spacecraft 1 and 4 than the pair was from each other. Due to this fact, it was not possible to rule out the possibility that the differences between spacecraft 3 and spacecraft 1 and 4 were due to distance. Since spacecraft 1 and 4 will ultimately be those used for the analysis of O^+, the coordinate system from spacecraft 3 will be ignored. Instead, the coordinate system calculated with spacecraft 4 will be used.

Space-craft	λ_L	λ_M	λ_N	λ_M/λ_N	***N* Vector** (in GSE)	$\lvert B_{L\ MAX}\rvert$ (nT)	$< B_N >$ (nT)	**Std. dev.** B_N (nT)
1	134	21.5	0.91	23.5	{0.72, -0.56, -0.40}	16	2.217	0.31
2	72.3	7.16	0.68	10.4	{0.38, -0.63, -0.68}	*N/A*[1]	*N/A*	*N/A*
3	147	12.3	0.23	52.6	{0.83, -0.45, -0.30}	~15	0.341	0.33
4	143	18.4	0.75	24.5	{0.74, -0.56, -0.36}	16	2.420	0.30

Table 1: Results of MVA per spacecraft for 2002-02-20 13:59:07-13:59:08 UT current sheet crossing. $|B_{L,MAX}|$ is the positive, maximum value the B_L component reaches on either side of the outflow region; $<B_N>$ is the average value of the normal component of the magnetic field in the outflow region; std. dev. B_N is the standard deviation of the normal magnetic field taken over the whole set of data points used in the MVA.

[1] Poor MVA results for SC2 did not allow for a meaningful estimation of the magnetic field strengths.

Spacecraft pair	$\Delta\varphi_L$	$\Delta\varphi_M$	$\Delta\varphi_N$	Spacecraft separation (km)
1 – 3	9.49°	6.49°	9.05°	179.6
1 – 4	0.53°	2.15°	2.14°	132.2
3 – 4	9.89°	4.85°	10.40°	209.9
2 – 1	3.01°	26.00°	26.13°	134.7
2 – 3	12.41°	32.06°	34.49°	125.7
2 – 4	2.54°	28.08°	28.19°	152.3

Table 2: Comparisons between the MVA systems calculated using each of the four spacecraft. Spacecraft pair indicates which spacecraft the comparison is being drawn between; $\Delta\varphi_i$ indicates the angular separation between the i coordinate axes of the pair.

Spacecraft 1 and 4 observed a similar, noticeably large normal component to the magnetic field. This is a strong indication that the local magnetopause is a rotational discontinuity. Spacecraft 3 observed a much smaller normal component, but the total strength of this field was comparable to the standard deviation of points so no conclusion can be drawn. The absolute value of B_L at the edges of the outflow region was included in Table 1, as this value can later be used with $< B_N >$ to generate an estimate of the reconnection rate as per Equation (4). An example of the electromagnetic fields in *LMN* is shown in Figure 19. The electric fields were used in *Vaivads et al.,* [2004] to help aid in the estimation of the reconnection rate. That study was performed on an earlier event on this same day. Here we have included the electric fields to demonstrate that this analysis is not possible in this event study due to large, pervasive data gaps for each of the three satellites EFW is active on.

In the time span shown in Figure 19, Cluster crossed the outflow region a total of three times. This is evidenced by (a) a sign change in $\vec{B}_L$ and (b) a reduction in $|\vec{B}_N|$ (see *Section* 3.6.2. Structure of the Magnetic Field, also Figures 6 and 7). There was no immediately obvious bipolar signature in $\vec{B}_M$ during these small, rapid crossings, possibly indicating that Cluster was far from the diffusion region (*Vaivads et al.,* [2004a, 2006b]).

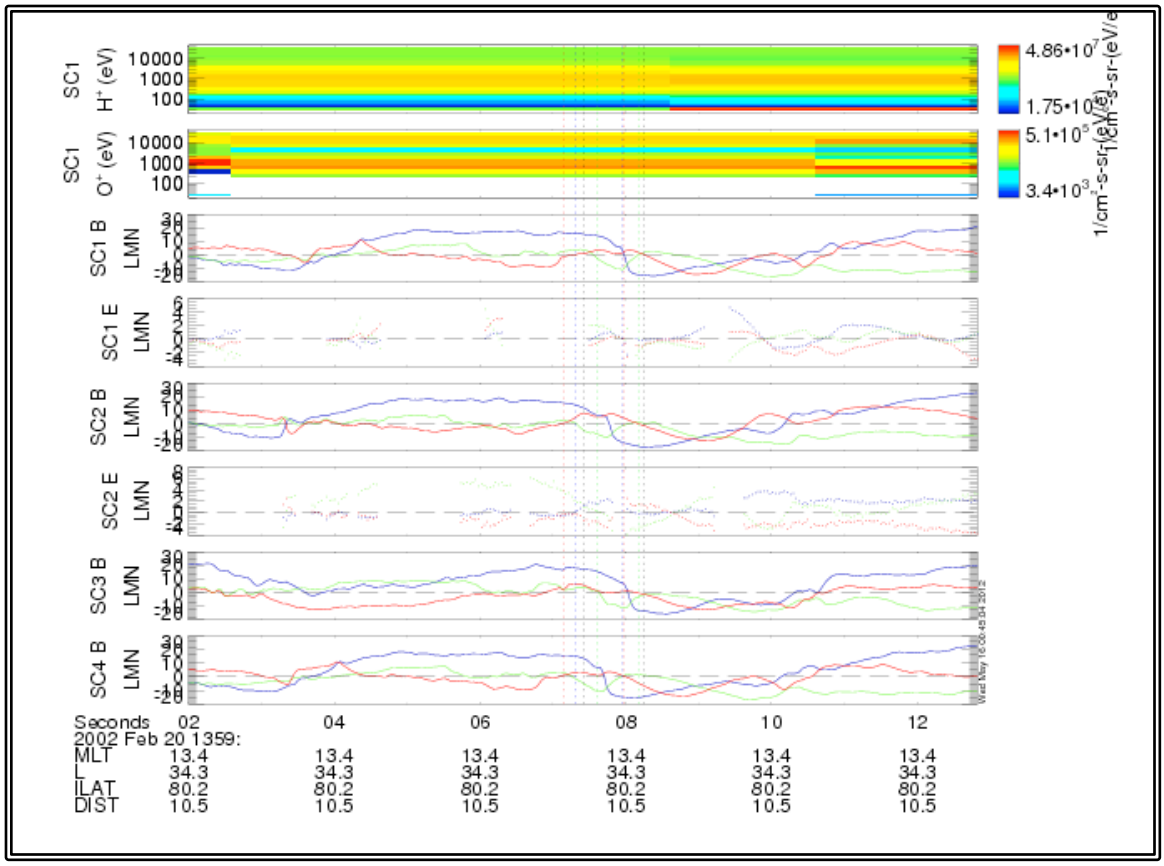

Figure 19: The electromagnetic fields in the calculated *LMN* coordinate system for each of the four cluster spacecraft. The vertical bars indicate where the MVA calculation is performed, where black indicates spacecraft 1, blue indicates spacecraft 2, green indicates spacecraft 3 and red indicates spacecraft 4. For the fields, the *L* component is shown in blue, the *M* component is shown in green and the *N* component is shown in red.

6.1.4. Quantitative Assessment of Jets with the Walén Test

The CODIF H^+ and O^+ differential flux spectra for spacecraft 1 have been included in Figure 19. This was done to show that the crossings of the reconnection region occurred on a much smaller time scale than that of the ion distributions from CODIF instrument. Most of the CODIF ion distributions were likely sampled from a mixture of plasmas in the separatrix, magnetosheath and reconnection outflow regions. Despite this inconsistent sampling, the jet-like signatures were still quite prominent. This was most likely due to the fact that the Cluster spacecraft did not stray far from the boundary region during 13:57:30 – 13:59:00 UT. It is highly possible that despite contamination from the separatrix and inflow regions, the

CODIF instrument was sampling ions from the outflow region during for such a fraction of the time to produce the noticeable flow enhancement observed in this interval.

The results of the Walén test and the deHoffmann-Teller analysis are shown in Figure 20 (described in *Sections* 5.4.2. The Walén Test for the Magnetopause as a Rotational Discontinuity and 5.4.3. Identifying the deHoffmann-Teller (dHT) Reference Frame). The test was performed using data points between 13:59:04 and 13:59:12 UT. The top panel of Figure 20 shows the fit for the measured convective electric field ($\vec{E}_C = \vec{v}_{CODIF} \times \vec{B}$) vs. the dHT predicted electric field ($\vec{E}_{dHT} = \vec{V}_{dHT} \times \vec{B}$). The fit for this comparison has a slope of 1.005 with a high correlation coefficient of approximately 1. The value of D/D_0 is 0.003, fitting the quality constraint $D/D_0 << 1$. All of these values indicate a high accuracy of the dHT frame.

The comparison of the measured and dHT velocities with the Alfvén velocity is shown in the bottom panel of Figure 20. The magnetosheath reference interval used for the calculation of the local Alfvén speed (as per Equation (6)) was 14:20:05 – 14:21:58 UT. Though the temporal separation between the jet (~13:58 UT) and the magnetosheath reference frame may seem large, the two intervals shared very similar IMF conditions (*Phan et al.,* [2004]). The slope of the fit shown on the bottom of Figure 20 is ~1.07. The fit had a correlation coefficient of 0.98. This shows that despite the possibility that contamination may have been present in these distributions, the bulk velocity is inarguably Alfvénic in speed and direction.

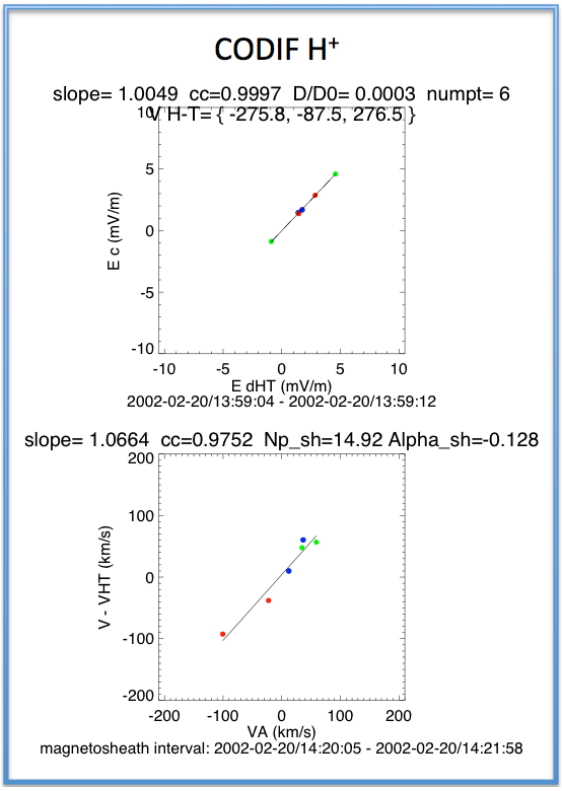

Figure 20: The results of deHoffmann-Teller and Walén analysis for the jet encountered at February 20, 2002 13:59 UT by Cluster 1.

6.1.5. Analysis of O+ Dynamics

Now that the Walén relation for H+ has been deduced, it is possible to draw a comparison between the local Alfvén speed in the dHT frame and the velocity of O+. Figure 21 shows the Alfvén speed (dashed blue line), the bulk velocity of H+ and the energy-limited bulk velocity of O+ averaged over the time interval given in Figure 20. The velocities are shown in the *LM* plane. The angular separation of the H+ velocity from the predicted velocity was >>1°. The angular separation of this pair of velocities from the O+ bulk velocity was also >>1°. The magnitude of the O+ velocity was approximately a factor of 0.2 less than the H+ / Alfvén velocity.

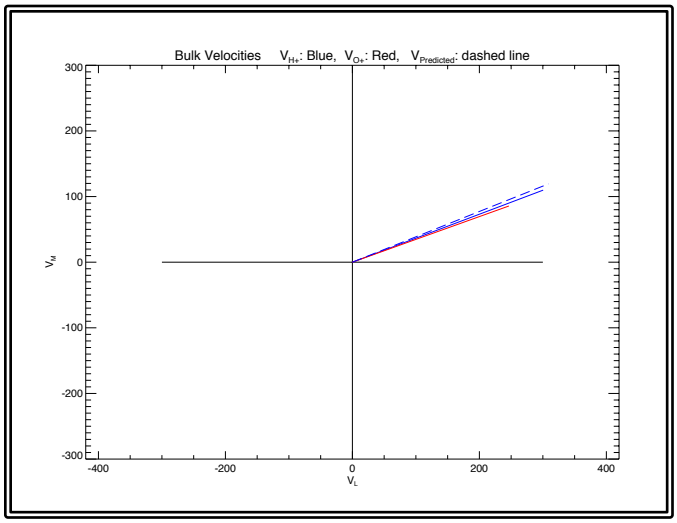

Figure 21: The bulk velocities of H^+ (blue solid line) and O^+ (red solid line), as well as the predicted velocity (blue dashed line) in the *LM* plane during the interval 2002-02-20 13:59:04 – 13:59:12 UT. Units of the axis are km/s, and the predicted velocity was determined using the Walén test (*Sonnerup et al.,* [1987], *Phan et al.,* [2001a, 2004]).

6.1.5. Estimation of Reconnection Rate

Using the method given in Equation (4) and the results of the minimum variance analysis for multiple spacecraft we were able to find an estimate for the normalized rate of reconnection. Table 3 gives these values.

	R_{NORM}
Spacecraft 1	0.1375
Spacecraft 3	0.1510
Spacecraft 4	0.0227
Average	0.103

Table 3: Estimation of the normalized reconnection rate for the 13:59 UT encounter with the reconnection jet. Estimated using Equation (4) and results from Table 1.

An average value of ~0.1 was deduced for the normalized rate of reconnection. This is identical to the value given in *Vaivads et al.,* [2004] for a Cluster encounter with magnetopause reconnection that happened approximately one hour prior to the 13:59 UT event.

6.2. January 4, 2004

6.2.1. Event Overview

During January 4th, 2004, between 12:30 and 14:30 UT Cluster observed several full and partial crossings of the magnetopause (see *Section* 5.4.1. Identifying Cluster Crossings of the Magnetopause). Cluster was located on the duskside, sunward of the cusp as shown in Figure 16. All four spacecraft were tightly spaced (≤300 km). Crossings of the magnetopause occurred between the magnetosheath and inner magnetosphere. Since the solar wind dynamic pressure was fairly constant throughout the event duration, the movement of the boundary is thought to have been driven by a propagating FTE located somewhere in the vicinity of Cluster (*Lindstedt et al.,* [2009]). A southward IMF B_z was observed throughout almost the entire duration of the event. Such a southward IMF is consistent with reconnection at the dayside magnetopause. Variations observed in the IMF B_y prevent a meaningful estimation of the IMF average clock angle. Using the T96 magnetospheric model, a positive B_y would be consistent with antiparallel reconnection at the duskside magnetopause. The geomagnetic activity during this time was low, as indicated by the DST index, suggesting that this was a non-storm time event. During this time the Cluster satellites were in burst mode, meaning the distributions of all ion species were available from the CODIF instruments with the highest telemetry possible. Figure 23 shows an overview of this event using Cluster and ACE data.

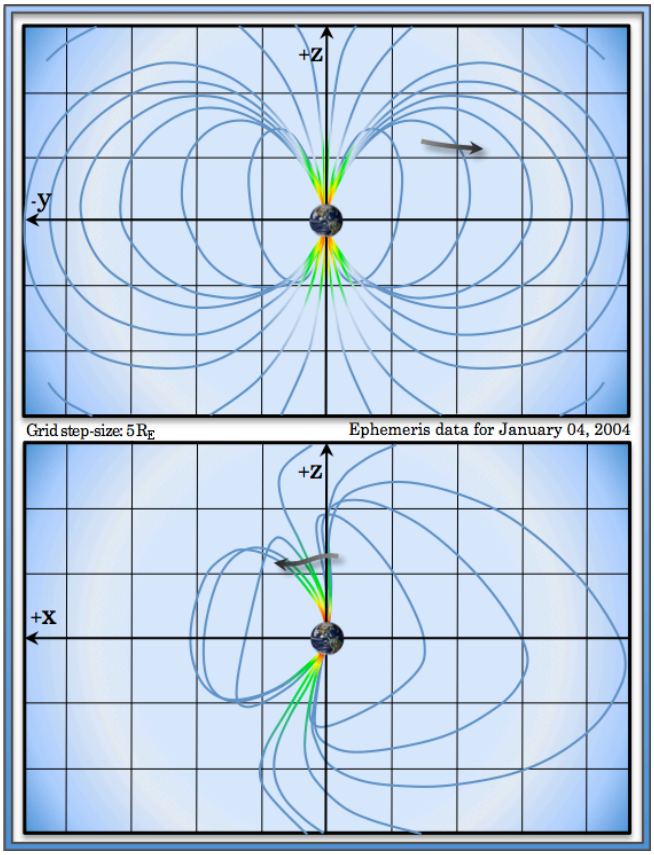

Figure 22: Ephemeris data for the Cluster satellites on January 4, 2004, from 12:00 to 15:00 UT. Made with the help of the Orbit Visualizer Tool (http://ovt.irfu.se/download.jsp).

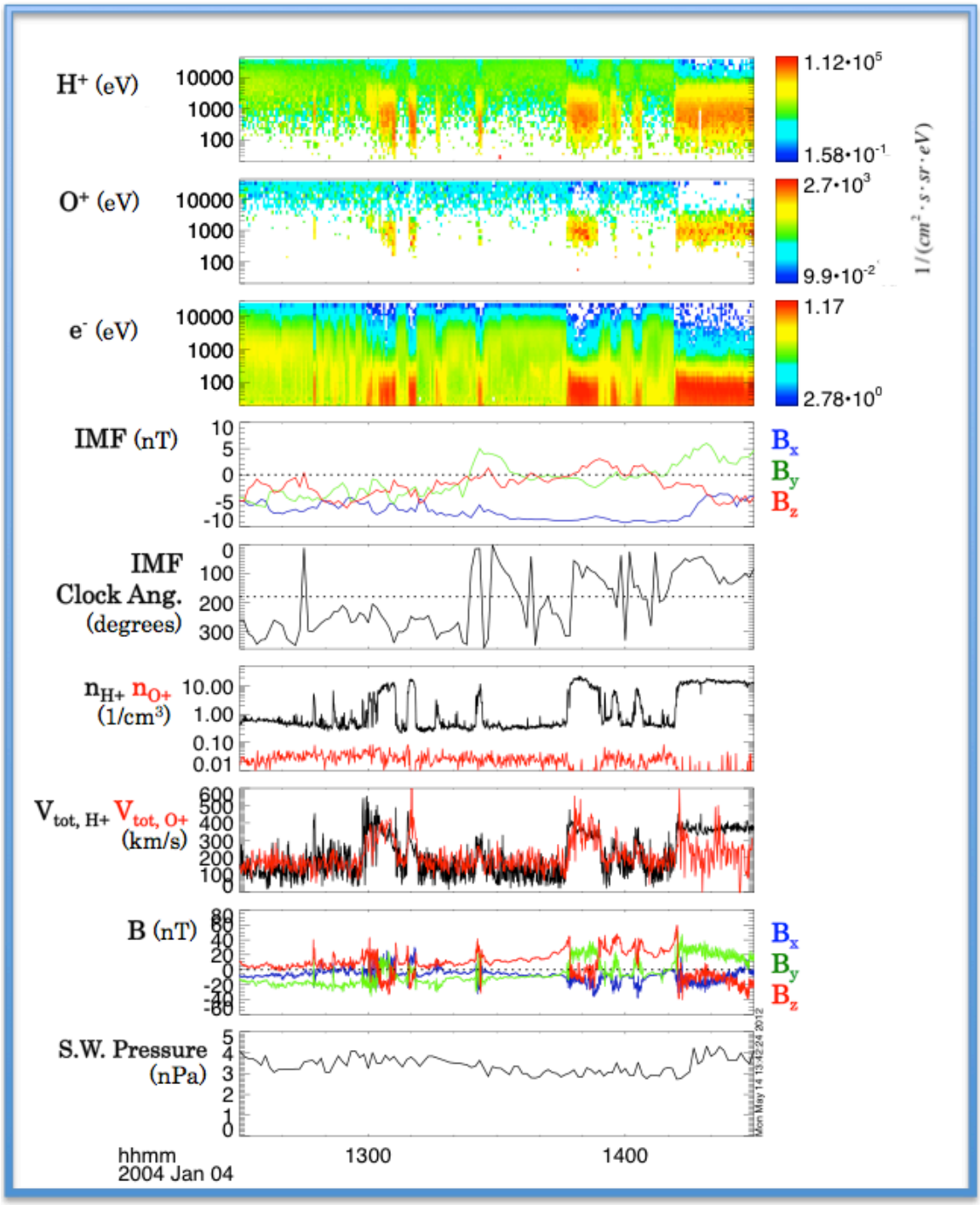

Figure 23: Overview of January 4, 2004 event with Cluster and ACE data.

Calibrations for this event were used for examples in *Section* 5.3.1. Saturation of Cluster-CODIF in High Count Rate Environments (Figure 10). The results of the cross-calibration of CODIF with HIA and WHISPER are shown in the next section,

5.3.2. Cross-Calibration Results of the High Rates Correction (Figure 11). Favorable comparisons between CODIF H^+ density and both WHISPER e^- and HIA H^+ densities were made in the magnetosheath post-calibration. H^+ spillover into the O^+ TOF channels was visible between the energies 300 eV and 5 keV. The energy range used to calculate all moments of the O^+ distributions was 5 keV – 40 keV.

During each crossing of the magnetopause, high energy O^+ was observed (~10 keV). The average number density of O^+ on the magnetospheric side of the magnetopause was ~0.03 cm^{-3} which is comparable to the density observed in the February, 2002 event. The number density ratio of H^+ to O^+ in the magnetosphere was considerably larger in this event, with an average value of ~25. The mass density ratio of H^+ to O^+ in the magnetospheric side of the magnetopause was ~1–1.5. For some crossings where Cluster traversed the magnetopause, O^+ was observed during the entire time the satellites were in the magnetosheath. This is expected to be due to the finite gyroradius effect, as no magnetospheric electrons are observed during these times. For some crossings, the bulk energy of the O^+ exceeded the upper bound of the energy window of CODIF. Observation of these events will be discussed in the following sections. This event was studied in *Khotyaintsev et al.,* [2006] and again in *Lindstedt et al.,* [2009]. Both studies provided rigorous analyzation of H^+ dynamics and the electromagnetic field structures within the reconnection region, but neither considered the dynamics of O^+.

6.2.2. Qualitative Assessment of Jets

In *Lindstedt et al.,* [2009] he identifies eight total Cluster encounters with magnetopause reconnection events. Of these eight, we will present detailed analysis of three. Figure 24 shows Cluster 1 CODIF, PEACE and magnetometer data for these three crossings. Here, Cluster begins in the magnetosheath and ends in the magnetosphere, traversing the magnetopause three times in between.

Of these three crossings, two events had the bulk energy of O^+ within the energy window of CODIF. For the third event, the bulk energy of O^+ was above the upper bound of the energy window. Note that for crossings (1) and (3) the perpendicular velocity of O^+ almost precisely matches that of H^+. In these events the

O^+ bulk energy was within the energy window of CODIF. For crossing 2 the bulk energy of O^+ was above the upper bound of the energy window of CODIF. For this crossing the perpendicular velocity of O^+ was slightly less than that of H^+. For all three crossings the total and parallel velocities of O^+ were less than that of H^+.

Figure 25 shows the Cluster 1 CODIF distribution function plots for H^+ and O^+ for the 13:06 UT jet encounter. Here Cluster crosses from the magnetosheath (panels (a) and (b)), into the jet region (panels (c) and (d)) and then into the magnetosphere (panels (e)and (f)). Note that in panel (b), while Cluster is in the magnetosheath, a small amount of O^+ content is observed at the 90° pitch angle line, indicating some small presence of finite gyroradius O^+. A large amount of O^+ is also observed streaming with magnetosheath flow, suggesting O^+ that escaped from the magnetosphere is behaving as a pickup ion. This crossing is depicted in Figure 24 and labeled as crossing (1).

Figure 26 shows the Cluster 1 CODIF distribution function plots for H^+ and O^+ for the 13:09 UT jet encounter. Here Cluster crosses from the magnetosphere (panels (a) and (b)), into the jet region (panels (c) and (d)) and then into the magnetosheath (panels (e)and (f)). Note that in panel (d), while Cluster is in the jet, a large amount of O^+ content is observed at the 90° pitch angle line at the upper bound of the energy window of CODIF. This suggests that any moments calculation being done with this distribution may not be accurate, as it does not include a fair amount of the distribution. This could explain the slower perpendicular flows of O^+ observed in Figure 24 crossing (2).

Figure 27 shows the Cluster 1 CODIF distribution function plots for H^+ and O^+ for the 13:11 UT crossing (labeled (3) in Figure 24). Here Cluster crosses from the magnetosheath (panels (a) and (b)), into the jet region (panels (c) and (d)) and then into the magnetosphere (panels (e)and (f)). In panel (b), taken to be the time-integrated distribution function O^+ in the magnetosheath, a noticeable distribution of O^+ is observed at ±90° pitch angle. This is understood to be finite gyroradius O^+. In panel (d) O^+ is observed streaming along the $+V_{par}$, $+V_{perp}$ direction. This is the relatively the same direction the H^+ is observed streaming along.

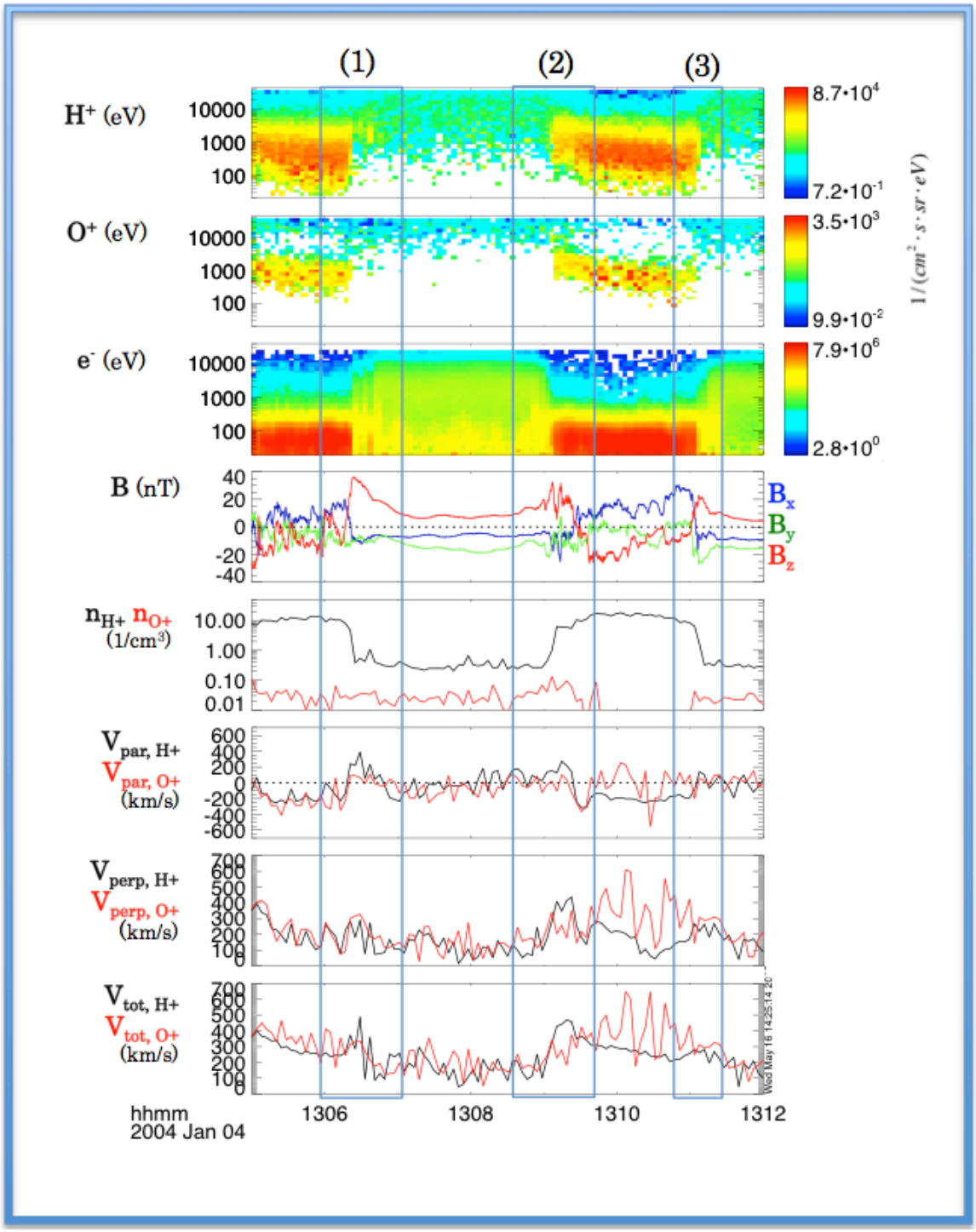

Figure 24: Three encounters with magnetopause reconnection observed by Cluster 1 on January 4, 2004.

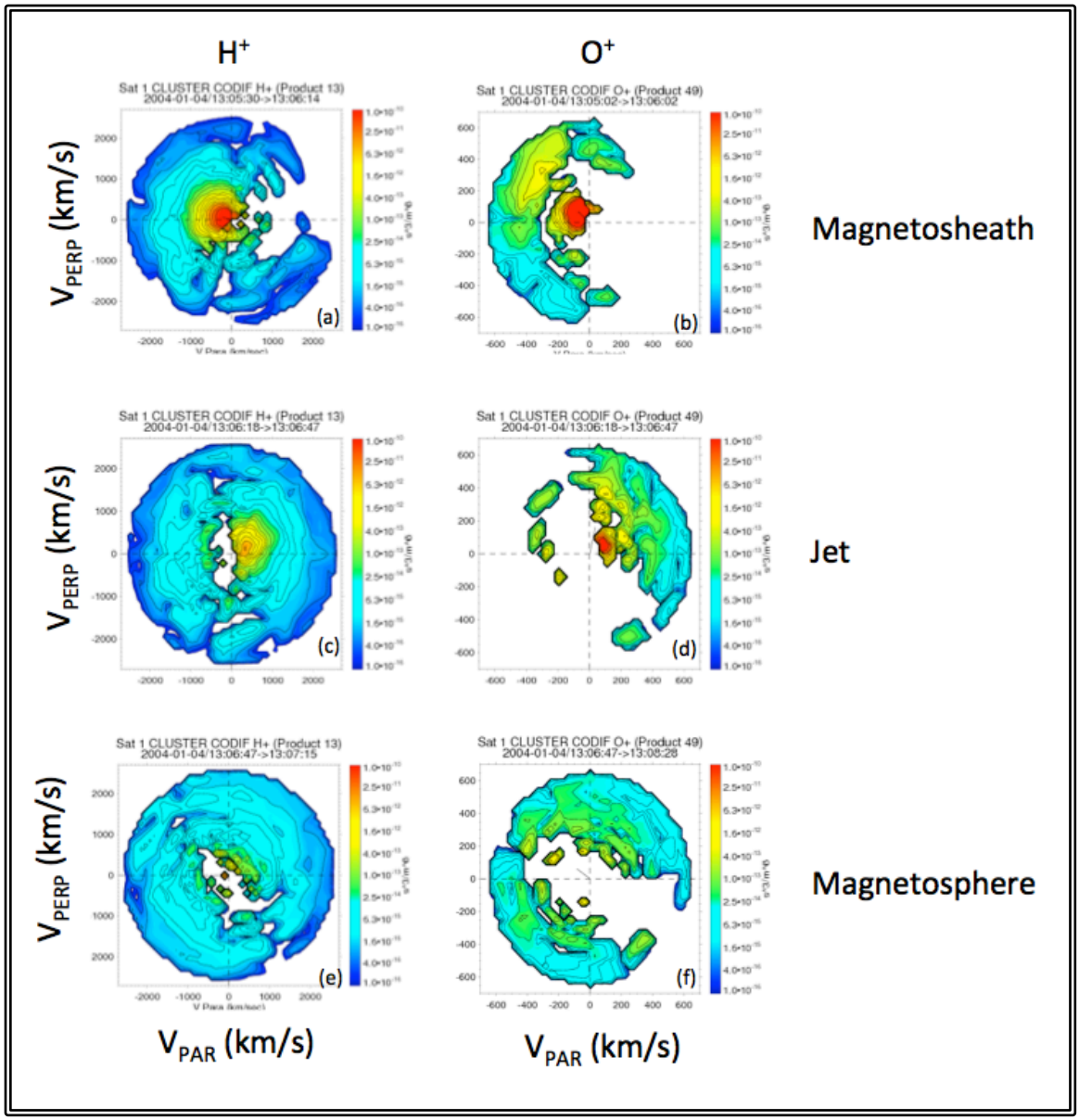

Figure 25: Distribution functions from Cluster-CODIF 1 taken before, during and after the encounter with the reconnection jet at 13:06 UT.

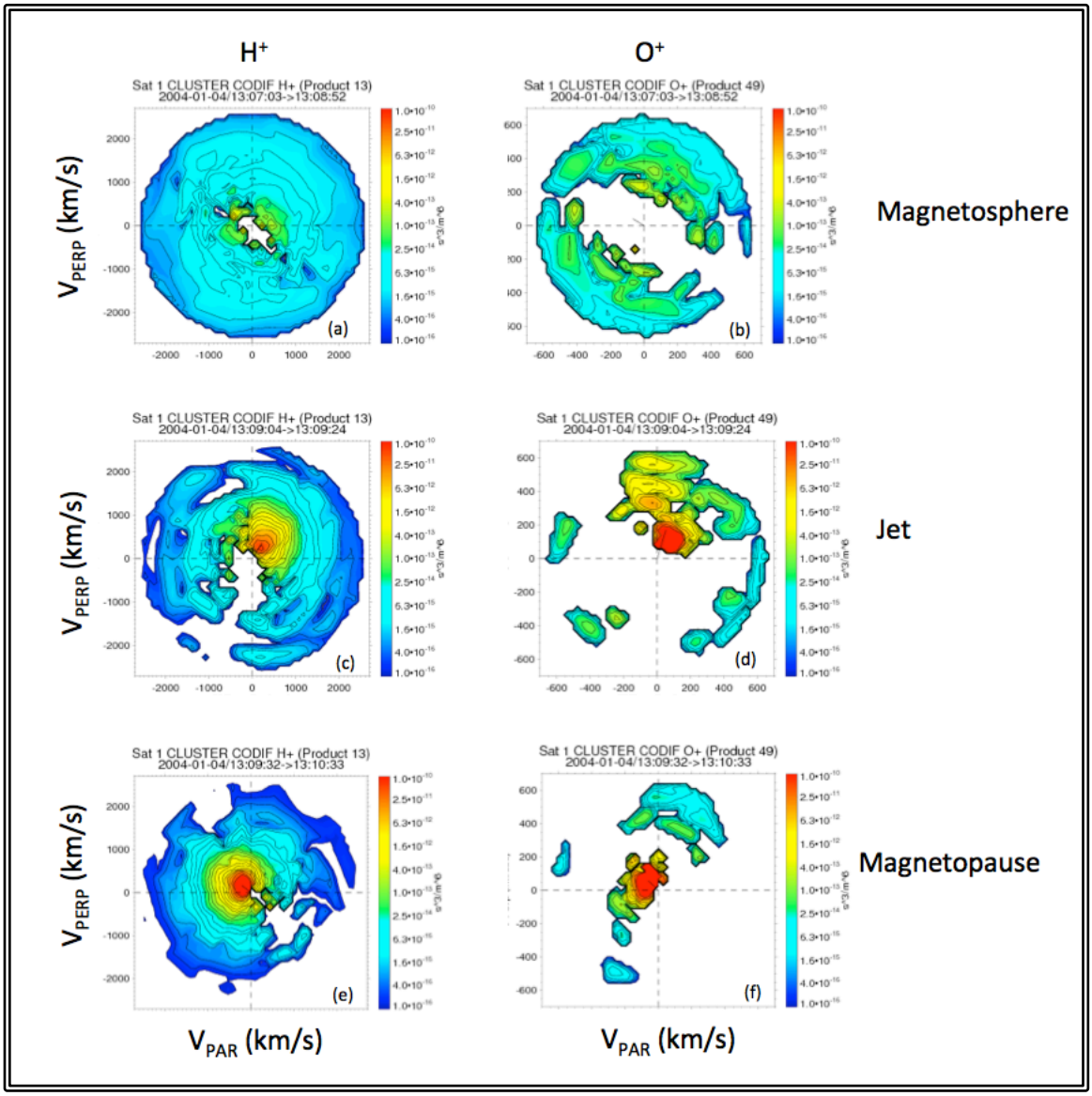

Figure 26: Distribution functions from Cluster-CODIF 1 taken before, during and after the encounter with the reconnection jet at 13:09 UT.

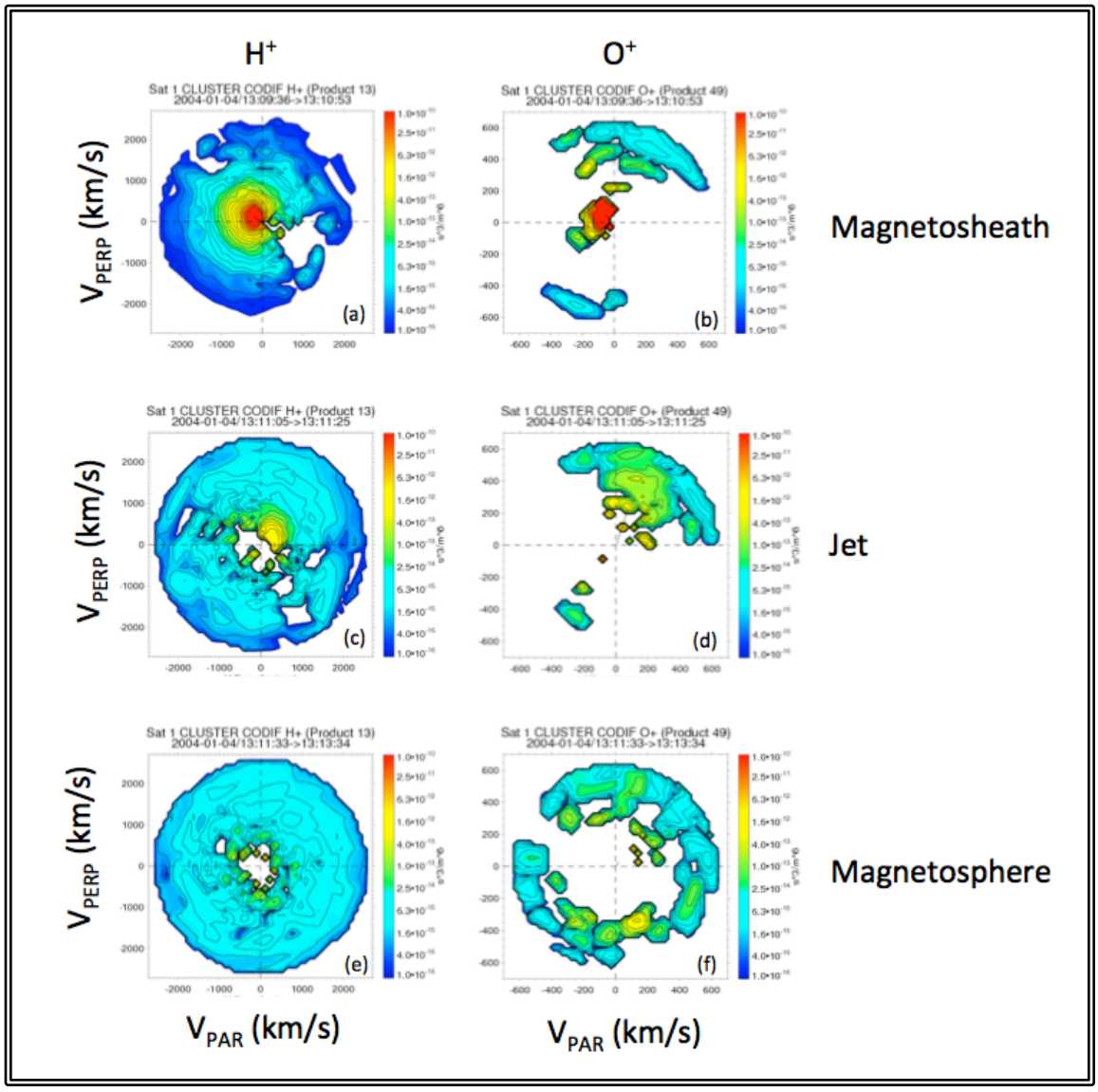

Figure 27: Distribution functions from Cluster-CODIF 1 taken before, during and after the encounter with the reconnection jet at 13:11 UT.

6.2.3. Minimum Variance Analysis Results

In *Lindstedt et al.,* [2009] he provides a MVA coordinate system for the jet at 13:11 UT. We will use this coordinate system as a reference here. Magnetometer data from spacecraft 1, 3 and 4 was used; we were unable to find an accurate MVA system from spacecraft 2. Table 3 contains the results and parameters from the MVA calculation for spacecraft 1, 3 and 4. Table 4 gives comparisons between these

three coordinate systems and the reference system from *Lindstedt et al.*, [2009]. A comparison of the coordinate systems is shown in Figure 28.

Space-craft	λ_L	λ_M	λ_N	λ_M/λ_N	***N* Vector** (GSE)	$\lvert B_{L\ MAX}\rvert$ (nT)	$< B_N >$ (nT)	**Std. dev. B_N** (nT)
1	1.93	0.22	0.008	28.9	{0.15, 0.64, 0.76}	25	3.25	0.39
3	10.8	1.49	0.101	13.9	{0.20, 0.67, 0.71}	14	3.61	0.77
4	12.7	1.88	0.021	87.7	{0.02, 0.58, 0.81}	12	0.048	0.33

Table 4: Results of MVA per spacecraft for the 2004-01-04 13:11 UT current sheet encounter.

Spacecraft pair	$\Delta\varphi_L$	$\Delta\varphi_M$	$\Delta\varphi_N$	**Spacecraft separation (km)**
1 – *Ref.*	15.3°	9.29°	12.2°	*N/A*
3 – *Ref.*	25.8°	28.9°	12.4°	*N/A*
4 – *Ref.*	23.8°	23.1°	13.9°	*N/A*
1 – 3	16.8°	16.2°	4.64°	237.0
1 – 4	15.1°	15.1°	8.56°	276.9
3 – 4	11.9°	7.19°	13.1°	276.0

Table 5: Comparisons between the MVA systems from three of the four Cluster spacecraft during the 2004-01-04 13:11 UT jet encounter. Also included are comparisons with the coordinate system given in *Lindstedt et al.,* [2009], denoted '*Ref.*' Here $\Delta\varphi_i$ denotes the angular separation between the two *i* coordinate axes of the pair of spacecraft.

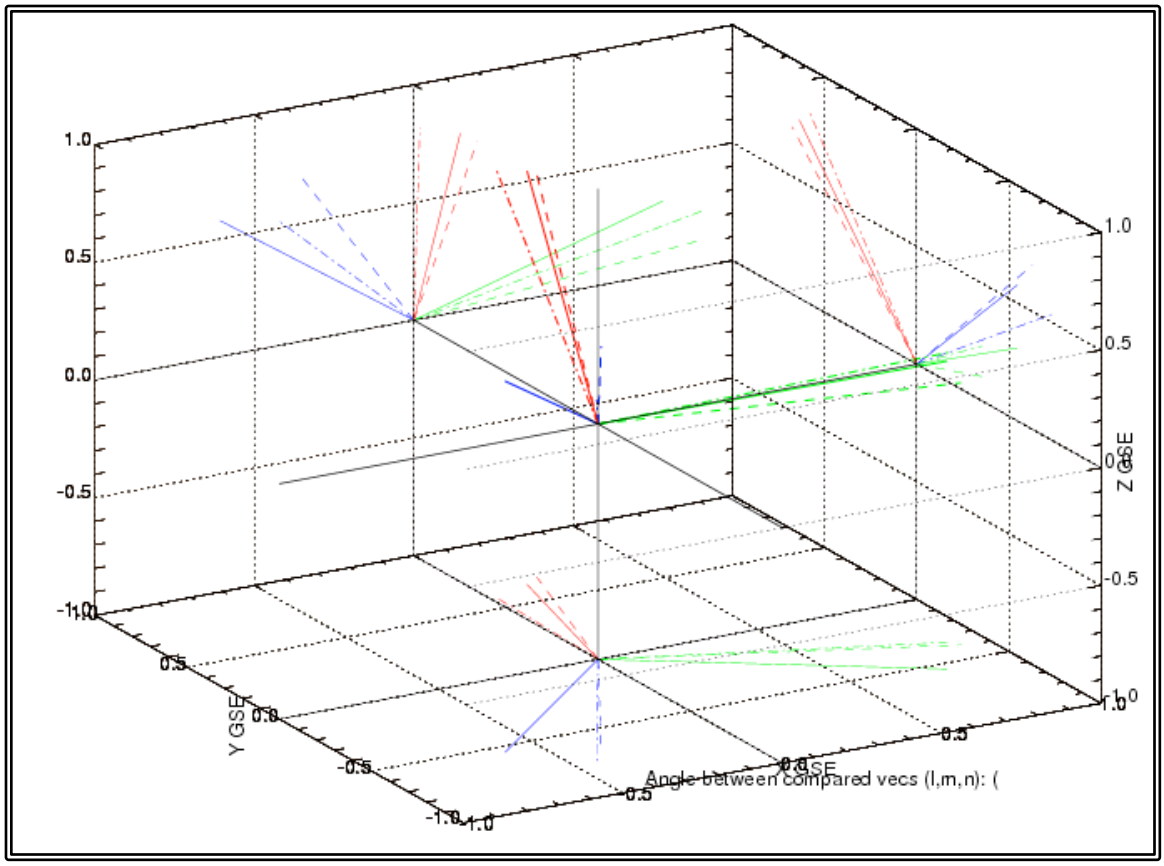

Figure 28: Comparisons of spacecraft 1, 3 and 4 MVA coordinate systems for the 2004-01-04 13:11 UT jet encounter. The *L* vector is shown in blue, the *M* in green and the *N* in red. The solid lines are the spacecraft 1 coordinate axis, the dashed lines are spacecraft 3 and the dash-dotted lines are spacecraft 4.

As evidenced by the angular difference between each coordinate system, there was no clear advantage gained from multi-spacecraft analysis. The comparison of the *LMN* coordinates do however confirm that the coordinate system is at least roughly accurate, as all of the three systems derived in this study are within at most 20° of one another. No coordinate system could be considered clearly superior by means of the comparison with the *Lindstedt et al.,* [2009] system. The MVA system from spacecraft 4 was chosen due to its high eigenvalue separation and low standard deviation in the normal magnetic field component.

MVA was performed on the 13:06 UT reconnection encounter. Here, a ~15° angular discrepancy between the systems of each of the four spacecraft was observed. However, it was noted that the directions of each of the axes of the 13:06

UT MVA system were within ≤15° of those calculated for the 13:11 UT system (comparison done using spacecraft 4 data). Since 15° seemed to be the typical angular separation of the vectors per spacecraft in the 13:11 UT event, these coordinates were deemed to be adequate to describe both the 13:06 and 13:09 jets.

6.2.4. Quantitative Assessment of Jets with the Walén Test

Figures 29, 30 and 31 show the results of the Walén test for a rotational discontinuity, as performed on the three jets shown in Figure 24. All three events displayed a nearly 1:1 ratio between the $V_{dHT} + v_A$ and the measured velocities indicating that these were all reconnection events. The result from the 13:11 UT jet is surprising than the others due to the very low B_N value measured by spacecraft 4 in the MVA coordinate system.

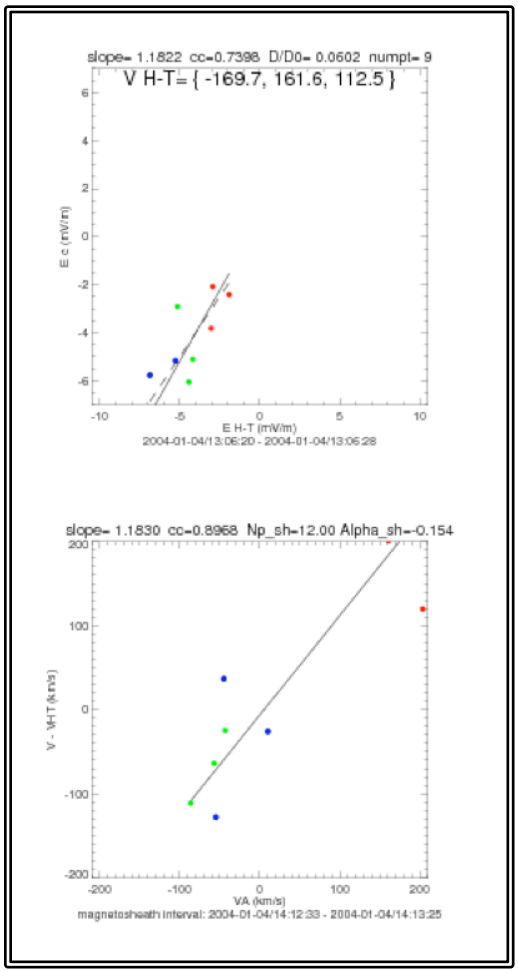

Figure 29: Results of Walén analysis on the Cluster 1 observation of the 13:06 UT jet.

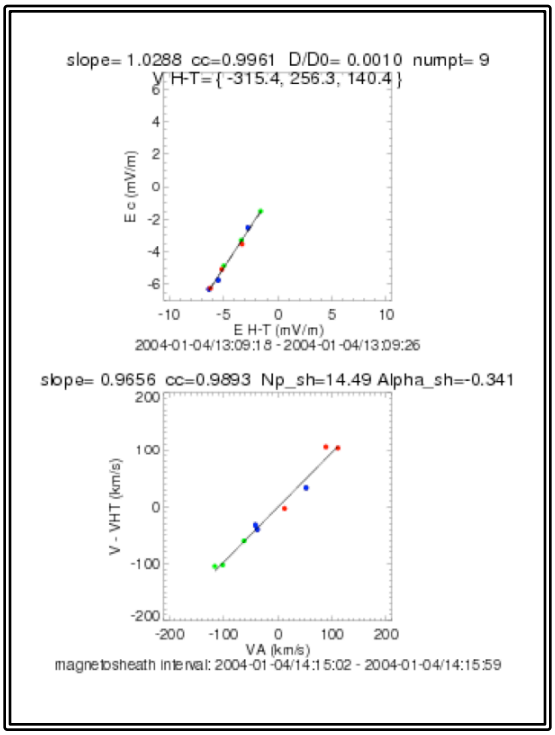

Figure 30: Results of Walén analysis on the Cluster 1 observation of the 13:09 UT jet.

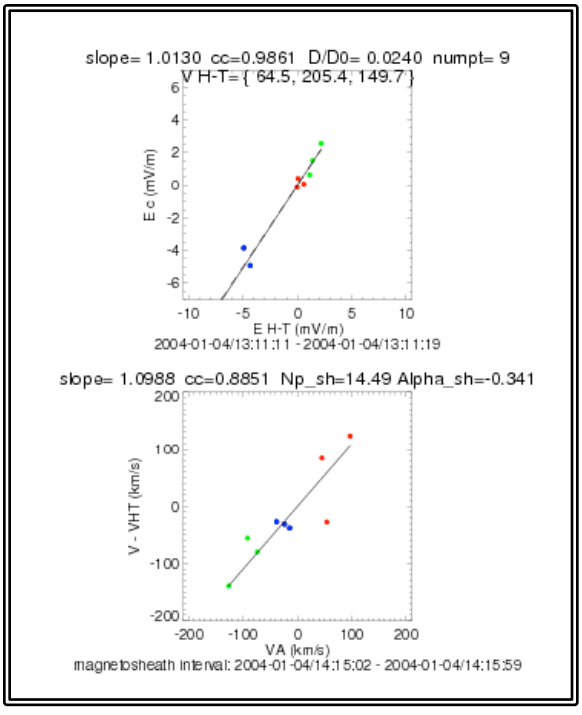

Figure 31: Results of Walén analysis of the Cluster 1 observation of the 13:11 UT jet.

6.2.6. Estimation of the Reconnection Rate

Using the method given in Equation (4) and the results of the minimum variance analysis for multiple spacecraft we were able to find an estimate for the normalized rate of reconnection. Table 6 gives these values.

	R_{NORM}
Spacecraft 1	0.13
Spacecraft 4	0.005
Average	0.07

Table 6: Estimations of the reconnection rate determined from minimum variance results of the 13:11 UT crossing. Spacecraft 3 was not included due to its large standard deviation in the B_N calculation.

As evidenced in Tables 4 and 5, the minimum variance system had larger error indicators than the previously studied event. It should be noted that these values given should only be interpreted as rough approximations. Since no MVA systems could be deduced for the 13:06 or 13:09 crossings, no meaningful estimation of the reconnection rate could be deduced for them.

6.2.5. Analysis of O+ Dynamics

Figures 32, 33 and 34 give comparisons between the bulk velocities of H^+ and O^+ as well as the predicted velocity of O^+ using the Walén relations deduced in the previous section. For each figure, the O^+ velocity is shown in red, the H^+ (measured) in solid blue and the H^+ (predicted) in dashed blue. For the jet at 13:06 UT, the bulk velocity of O^+ was separated by ~30° angular difference in the *LM* plane. The O^+ velocity vector was a factor of 0.1 smaller than that of H^+. For the jet at 13:09 UT, the bulk velocity of O^+ was separated by that of H^+ by 22°. The O^+ velocity vector was a factor of 0.4 smaller than the H^+ velocity. Due to the fact that some of the perpendicular distribution of O^+ may have been out of the energy range of CODIF, a larger separation of the pair of vectors in the normal direction would be expected. Finally, for the last jet at 13:11 UT, the O^+ velocity was separated by 5° from the H^+ velocity in the *LM* plane. Surprisingly, O^+ was observed streaming at a velocity a factor of 1.7 larger in magnitude than the H^+ velocity. It is possible that the

distributions used in this comparison may have included some sampling of the separatrix or inflow regions.

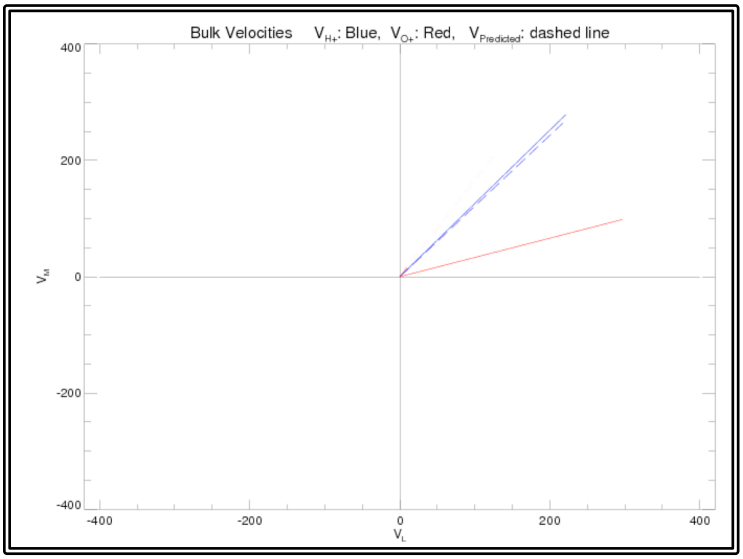

Figure 32: Comparison of O^+, H^+ and predicted H^+ bulk velocities during the interval 2004-01-04 13:06:20 – 13:06:28 UT. Comparison drawn with Cluster 1 data compared using the coordinate system deduced in the Minimum Variance Analysis section. Units here are in km/s.

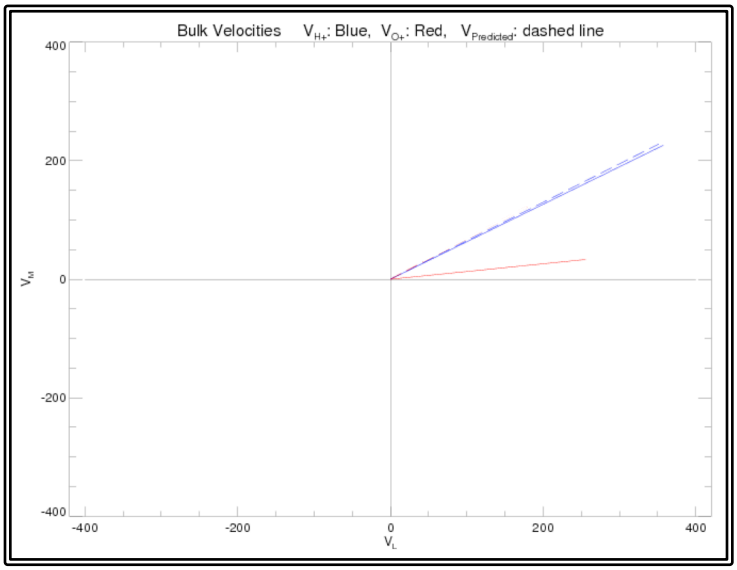

Figure 33: Comparison of O^+, H^+ and predicted H^+ bulk velocities during the interval 2004-01-04 13:09:18 - 13:09:26 UT. Comparison is drawn with Cluster 1 data compared using the coordinate system deduced in the Minimum Variance Analysis section. Units here are km/s.

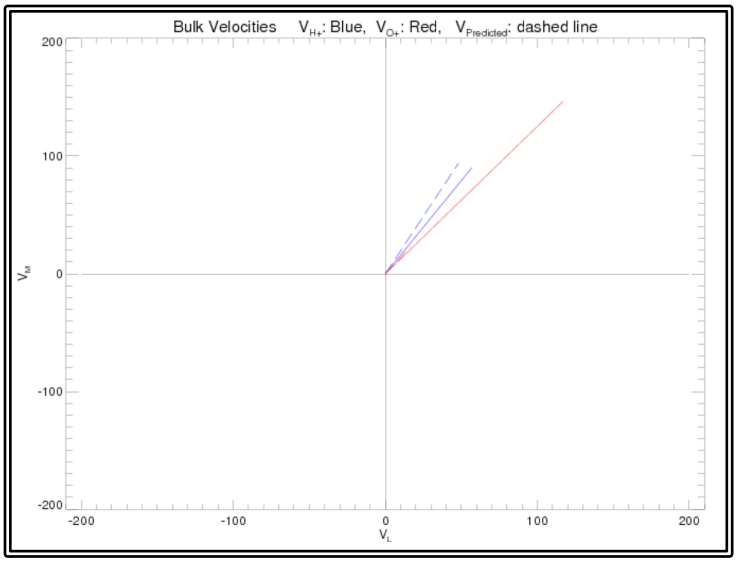

Figure 34: Comparison of O^+, H^+ and predicted H^+ bulk velocities during the interval 2004-01-04 13:11:11 - 13:11:19 UT. Comparison is drawn with Cluster 1 data compared using the coordinate system deduced in the Minimum Variance Analysis section. Units here are km/s.

7. Concluding Remarks and Future Goals

Our conclusion is that for each of the four events studied, O^+ was observed roughly following the direction of H^+ indicating that O^+ was at least partially magnetized in the reconnection outflow regions. In the 2002-02-20 13:59 UT jet, O^+ was almost certainly fully magnetized in the reconnection region. In the three jets from the 2004-01-04 event, the conclusions vary. For the first jet (13:06 UT) the velocity of O^+ has a large angular separation from that of H^+ in the *LM* plane. It was observed convecting at a perpendicular velocity almost identical to H^+ however, indicating that O^+ was at least partially magnetized to the inflow and outflow fields (Figure 24). This conclusion is supported by observations of the O^+ distribution function during the jet encounter (Figure 25). O^+ is *not* streaming at a ±90° pitch angle, indicating that it is not simply finite gyroradius O^+. For the second jet, observed at 13:09 UT, no noticeable energy cut-off was observed to occur in the O^+ distribution (Figure 26). This suggests that the moments calculation performed with O^+ may not include the complete distribution. Very specifically, the moments may be missing high energy O^+ at a ~90° pitch angle. This is observed in Figure 24. For the last jet observed at 13:11, O^+ was observed at a much larger velocity than that of H^+, indicating that the distributions used to calculate the velocity moments may have included some contamination from plasma outside the outflow region. Despite this, O^+ is observed streaming at a direction roughly 5° away from the direction of H^+ indicating that O^+ is most likely entirely magnetized in this crossing.

The reconnection rate was also estimated, using the relation $R_{NORM} = B_L / B_N$. These estimations were very rough. In the future, analysis will be done using the same method of calculation but with timing analysis used to define the *LMN* system as this will most likely prove the more accurate method. The method proposed by *Fuselier et al.,* [2005] for calculation of the reconnection rate will also be tested. The goal of this will be to deduce the effect that O^+ has on the reconnection rate.

Another future goal is to deduce the reconnection structure / width of the reconnection region. We will do this to see if O^+ has any effect on the structure, then

compare to the theoretical / simulation evidence. One method of doing this is by using Equation (1) to deduce the gyroradius of O^+ in the magnetosheath. By using the lower bound of the energy of finite gyroradius O^+ in Equation (1), we can estimate an upper bound on the width of the reconnection region. Such finite gyroradius O^+ was observed in almost every crossing of the magnetopause.

In conclusion: despite the large gyroradius of high energy magnetospheric O^+, we have identified four Cluster encounters with magnetopause reconnection where O^+ is observed as being at least partially magnetized, if not fully magnetized. This result was determined from four out of the four events studied.

8. References

A., Balogh, M.W. Dunlop, S.W.H. Cowley, D.J. Southwood, J.G. Thomlinson, and the Cluster Magnetometer Team. "The Cluster Magnetic Field Investigation." *Space Science Review* 79 (1997): 65-91.

Berchem, J., and C.T. Russell. "The Thickness of the Magnetopause Boundary Layer: ISEE 1 and 2 Observations." *Journal of Geophysical Research* 87, no. A4 (1982).

Borovsky, Joseph E., Michael Hesse, Joachim Birn, and Maria M Kuznetsova. "What Determines the Reconnection Rate at the Dayside Magnetosphere?" *Journal of Geophysical Research* 113, no. A07210 (2007).

Bouhram, M., B. Klecker, G. Paschmann, S. Haaland, H. Hasagawa, H. Reme, J.-A. Sauvaud, L.M. Kistler, A. Balogh. "Survey of energetic O+ ions near the dayside mid-latitude magnetopause with Cluster." *Annales Geophysicae* 23 (2005): 1281-1294.

Cassak, P. A., and M. A. Shay. "Scaling of Asymmetric Magnetic Reconnection: General Theory of Collisionless Simulations." *Physics of Plasmas* 14, no. 102114 (2007).

Cassak, P. M., and M. A. Shay. "Scaling of Asymmetric Hall Magnetic Reconnection." *Geophysical Research Letters* 35, no. 19102 (2008).

Chaston, C.C., et al. "Drift-Kinetic Alfvén Waves Observed Near a Reconnection X Line in the Earth's Magnetopause." *Physical Review Letters* 95, no. 065002 (2005).

Crooker, S.W.H. "Dayside Merging and Cusp Geometry." *Journal of Geophysical Research* 84, no. 951 (1979).

Dungey, J.W. "Interplanetary Magnetic Field and the Auroral Zones." *Physical Review Letters* 6 (1961): 47-49.

Eastwood, J.P., et al. "Multi-Point Observations of the Hall Electromagnetic Field and Secondary Island Formation During Magnetic Reconnection." *Journal of Geophysical Research* 112, no. A06235 (2007).

Fuselier, S.A., K.J. Trattner, and S.M. Petrinec. "Antiparallel and Component Reconnection at the Dayside Magnetopause ." *Journal of Geophysical Research* 116, no. A10227 (2011).

Fuselier, S.A., K.J. Trattner, S.M. Petrinec, C.J. Owen, and H. Reme. "Computing the Reconnection Rate at the Earth's Magnetopause Using Two Spacecraft Observations." *Journal of Geophysical Research* 110, no. A06212 (2005).

Fuselier, S.A., S.M. Petrinec, and K.J. Trattner. "Antiparallel Magnetic Reconnection Rates at the Earth's Magnetopause." *Journal of Geophysical Research* 115, no. A10207 (2010).

Gosling, J.T., M.F. Thomsen, S.J. Bame, T.G. Onsager, and C.T. Russell. "The Electron Edge of the Low Latitude Boundary Layer During Accelerated Flow Events." *Geophysical Review Letters* 17 (1990): 1833-1836.

Gustafsson, G., Andre´, M., Carozzi, T., Eriksson, A. I., Fa¨lthammar, C.-G., Grard, R., Holmgren, G., Holtet, J. A., Ivchenko, N., Karlsson, T., Khotyaintsev, Y., Klimov, S., Laakso, H., Lindqvist, P.-A., Lybekk, B., Marklund, G., Mozer, F., Mur- sula, K., Pedersen, A., Popielawska, B., Savin, S., Stasiewicz, K., Tanskanen, P., Vaivads, A., and Wahlund, J.-E.

"First Results of Electric Field and Density Observations by Cluster EFW Based on Initial Month of Operation." *Annales Geophysicae* 19 (2001): 1219-1240.

Hesse, M., and J. Birn. "On the Cessation of Magnetic Reconnection." *Annales Geophysicae* 22 (2004): 603-612.

Hughes, W.J. "The Magnetopause, Magnetotail, and Magnetic Reconnection." By M.G. Kivelson and C.T. Russell, edited by M.G. Kivelson and C.T. Russell. Cambridge: Press Syndicate of the University of Cambridge, 1995.

ISSI/ESA. *Analysis Methods for Multi-Spacecraft Data.* Edited by Götz Paschmann and Patrick W. Daly. International Space Science Institute, 2000.

Johnstone, A. D., Alsop, C., Burge, S., Carter, P. J., Coates, A. J., Coker, A. J., Fazakerley, A. N., Grande, M., Gowen, R. A., Gur- giolo, C., Hancock, B. K., Narheim, B., Preece, A., Sheather, P. H., Winningham, J. D., and Woodliffe, R. D. "Peace: a Plasma Electron and Current Experiment." *Space Science Review* 79 (1997): 351-398.

Johnstone, A.D., et al. "Peace: a Plasma Electron and Current Experiment." *Space Science Review* 79 (1997): 351-398.

Karimabadi, H., V. Roytershteyn, C.G. Mouikis, L.M. Kistler, and W. Daughton. "Flushing Effect in Reconnection: Effect of Minority Species of Oxygen Ions." *Planetary and Space Science* 59, no. 7 (2011).

Kasahara, S., et al. "Escape of High-Energy Oxygen Through Magnetopause Reconnection Under Northward IMF." *Annales Geophysicae* 26, no. 395503966 (2008).

Kawano, H., and T. Higuchi. "A Generalization of the Minimum Variance Method." *Annales Geophysicae* 14, no. 10 (1996).

Kawano, H., and T. Higuchi. "The Bootstrap Method in Space Physics: Error Estimation for the Minimum-Variance Analysis." *Geophysical Research Letters* 22, no. 307 (1995).

Khotyaintsev, Yu. V., A. Vaivads, A. Retino, M. Andre, C.J. Owen, and H. Nilsson. "Formation of Inner Structure of a Reconnection Separatrix Region." *Physical Review Letters* 97, no. 205003 (2006).

Kistler, L.M., et al. "Contribution of Nonadiabatic Ions to the Cross-Tail Current in an O+ Dominated Thin Current Sheet." *JGR* 110, no. A06213 (2005).

Kivelson, M.G. "Physics of Space Plasmas." In *Introduction to Space Physics*, edited by M.G. Kivelson and C.T. Russell, 27-53. Cambridge: Press Syndicate of the University of Cambridge, 1995.

Levy, R.H., H.E. Petschek, and G.L. Siscoe. "Aerodynamic Aspects of the Magnetospheric Flow." *AIAA* 2, no. 12 (1964).

Lin, Y., and L.C. Lee. "Reconnection Layer at the Flank Magnetopause in the Presence of a Shear Flow." *Geophysical Research Letters* 21 (1994): 855-858.

Lindstedt, T., et al. "Separatrix Regions of Magnetic Reconnection at the Magnetopause." *Annales Geophysicae* 27, no. 4039-4056 (2009).

Liu, Y. "Heavy Ion Effects on Magnetic Reconnection in the Earth's Magnetotail." PhD Thesis Proposal, Physics Department and Space Science Center, University of New Hampshire, Durham, 2012.

Lockwood, M., and M.F. Smith. "Earth's Magnetospheric Cusps." *Rev. Geophys.* 34, no. 233 (1996).

Luhmann, J.G. "Ionospheres." In *Introduction to Space Physics*, by M.G. Kivelson and C.T. Russell, edited by M.G. Kivelson and C.T. Russell, 183-202. Cambridge: Press Syndicate of the University of Cambridge, 1995.

Möbius, E., et al. *The 3-D Plasma Distribution Function Analyzers with Time-of-Flight Mass Discrimination for Cluster, FAST and Equator-S.* Vol. 102, in *Measurement Techniques in Space Plasmas: Particles, Geophysical Monograph Series*, edited by F. Pfaff, E. Borovsky and T. Young, 243-248. Washington D.C.: American Geophysical Union, 1998.

Marcucci, M.F., et al. "Magnetospheric Oxygen in the Magnetosheath and its Response to IMF Orientation: Cluster Observations." *Journal of Geophysical Research* 109, no. A07203 (2004).

McCarthy, M.P., and J.P. McFadden. *Measurement of 0-25 eV Ions with a Retarding Potential Analyzer on the Cluster Ion Spectroscopy Experiment.* Vol. 102, in *Measurement Techniques in Space Plasmas: Particles, Geophysical Monograph Series*, edited by F. Pfaff, E. Borovsky and T. Young, 97-103. Washington D.C.: American Geophysical Union, 1998.

McComas, D.J., Bame, S.J., P. Barker, W.C. Feldman, J.L. Phillips, P. Riley, and J.W. Griffee. "Solar Wind Electron Proton Alpha Monitor (SWEPAM) for the Advanced Composition Explorer." *Space Science Review* 86 (1998): 563-612.

Mouikis, C.G., L.M. Kistler, Y.H. Liu, B. Klecker, A. Korth, and I. Dandouras. "H+ and O+ Content of the Plasma Sheet at 15-19 Re as a Function of Geomagnetic and Solar Activity." *Journal of Geophysical Research* 115 (2010).

Mozer, F.S., and A. Retino. "Quantitative Estimates of Magnetic Field Reconnection Properties from Electric and Magnetic Field Measurements." *Journal of Geophysical Research* 112, no. A10206 (2007).

NASA. *TWINS A & B.* Edited by Ruth Netting. Feb. 14, 2012. http://science.nasa.gov/missions/twins/ (accessed May 6, 2012).

Paschmann, G., et al. "Plasma Acceleration at the Earth's Magnetopause: Evidence for Reconnection." *Nature* 282 (1979): 243-246.

Pederson, A., et al. "Electron Density Measurements Derived from Spacecraft Potential Measurements on Cluster in Tenuous Plasma." *Journal of Geophysical Research* 113, no. 7 (2008).

Petschek, H.E. "Magnetic Field Annihilation." Edited by W.N. Hess. *The Physics of Solar Flares*, 1964.

Phan, T.D., et al. "Cluster Observations of Continuous Reconnection at the Magnetopause under steady Interplanetary Magnetic Field Conditions." *Annales Geophysicae* 22 (2004): 2355-2367.

Phan, T.D., et al. "Simultaneous Cluster and IMAGE Observations of Cusp Reconnection and Auroral Proton Spot for Northward IMF." *Geophysical Research Letters* 30, no. 10 (2003).

Rème, H., Aoustin, C., Bosqued, J. M., Dandouras, I., Lavraud, B., Sauvaud, J. A., Barthe, A., Bouyssou, J., Camus, Th., Coeur-Joly, O., Cros, A., Cuvilo, J., Ducay, F., Garbarowitz, Y., Medale, J. L., Penou, E., Perrier, H., Romefort, D., Rouzaud, J., Vallat, C., Alcaydé, D.,

Jacquey, C., Mazelle, C., d'Uston, C., Möbius, E., Kistler, L. M., Crocker, K., Granoff, M., Mouikis, C., Popecki, M., Vosbury, M., Klecker, B., Hovestadt, D., Kucharek, H., Kuenneth, E., Paschmann, G., Scholer, M., Sckopke, N., Seidenschwang, E., Carlson, C. W., Curtis, D. W., Ingraham, C., Lin, R. P., McFadden, J. P., Parks, G. K., Phan, T., Formisano, V., Amata, E., Bavassano-Cattaneo, M. B., Baldetti, P., Bruno, R., Chionchio, G., Di Lellis, A., Marcucci, M. F., Pallocchia, G., Korth, A., Daly, P. W., Graeve, B., Rosenbauer, H., Vasyliunas, V., McCarthy, M., Wilber, M., Eliasson, L., Lundin, R., Olsen, S., Shelley, E. G., Fuselier, S., Ghielmetti, A. G., Lennartsson, W., Escoubet, C. P., Balsiger, H., Friedel, R., Cao, J.-B., Kovrazhkin, R. A., Papamastorakis, I., Pellat, R., Scudder, J., Sonnerup, B. "First multispacecraft ion measurements in and near the earth's magnetosphere with the identical Cluster Ion Spectrometry (CIS) experiment." *Annales Geophysicae* 19, no. 1303-1354 (2001).

Retino, A., et al. "Structure of the Separatrix Region Close to a Magnetic Reconnection X-line: Cluster Observations ." *Geophysical Research Letters* 33, no. L06101 (2006).

Russell, C.T., and R.C. Elphic. "ISEE Observations of Flux Transfer Events at the Dayside Magnetopause." *Geophysical Research Letters* 6, no. 33 (1979).

Scudder, J.D., P.A. Puhl-Quinn, F.S. Mozer, K.W. Ogilvie, and C.T. Russell. "Generalized Walén Tests Through Alfvén Waves and Rotational Discontinuities Using Electron Flow Velocities." *Journal of Geophysical Research* 104, no. A9 (September 1999): 19,817-19,833.

Shay, M.A., and M. Swisdak. "Three Species Collisionless Reconnection: Effect of O+ on Magnetotail Reconnection." *Physical Review Letters* 93, no. 17 (2008).

Smith, C.W., L'Heureux J., N.F. Ness, M.H. Acuna, L.F. Burlaga, and J. Scheifele. "The ACE Magnetic Fields Experiment." *Space Science Review* 86 (1998): 613-632.

Sonnerup, B. U. Ö., I. Papamastorakis, G. Paschmann, and H. Lühr. "The Magnetopause for Large Magnetic Shear: Analysis of Convection Electric Fields from AMPTE/IRM." *Journal of Geophysical Research* 95 (1990): 10,541–10,557.

Sonnerup, B.U.O. "Magnetic Field Reconnection." Edited by L.T. Lanzerotti, C.F. Kennel and E.N. Parker. *Solar System Plasma Physics* III (1979): 47–108.

Sonnerup, B.U.O. "On the Stress Balance in Flux Transfer Events." *Journal of Geophysical Research* 92, no. A8 (1987).

Sonnerup, B.U.O., and Jr.,L.J. Cahill. "Explorer 12 Observations of the Magnetopause Current Layer ." *Journal of Geophysical Research* 73, no. 1757 (1968).

Sonnerup, B.U.O., et al. "Evidence for Magnetic Field Reconnection at the Earth's Magnetopause." 86, no. A12 (1981).

Trattner, K.J., J.S. Mulcock, S.M. Petrinec, and S.A. Fuselier. "Probing the Boundary Between Antiparallel and Component Reconnection During Southward Interplanetary Magnetic Field Conditions." *Journal of Geophysical Research* 112, no. A08210 (2007).

Tsyganeko, N.A. "Modeling the Earth's Magnetospheric Magnetic Field Confined Within a Realistic Magnetopause." *Journal of Geophysical Research* 100 (1995): 5599-5612.

Vaivads, A., A. Retino, and M. Andre. "Microphysics of Magnetic Reconnection." *Space Science Reviews* 112 (2006): 19-27.

Vaivads, A., et al. "Structure of the Magnetic Reconnection Diffusion Region from Four-Spacecraft Observations." *Physical Review Letters* 93, no. 10 (2004).

Wygant, J.R., et al. "Cluster Observations of an Intense Normal Component of the Electric Field at a Thin Reconnecting Current Sheet in the Tail and its Role in the Shock-Like Acceleration of the Ion Fluid into the Separatrix Region ." *Journal of Geophysical Research* 110 , no. A09206 (2005).

Zong, Q.-G., Wilken, B., et al. "Ring Current Oxygen Ions Escaping into the Magnetosheath." *Journal of Geophysical Research* 106 (2001): 25541-25546.

9. Acknowledgements

Special thanks to Chris Mouikis and Lynn Kistler for *patiently* teaching me everything from "what is plasma and why is it in space" to "how the cusp O^+ outflow is dependent on the F10.7 and Kp indices". After only four years, I finally *almost* understand how the plasma got into space.